Understanding the neutron noise induced by fuel assembly vibrations in linear theory

Annals of Nuclear Energy 175 (2022) 109169

Contents lists available at ScienceDirect

Annals of Nuclear Energy

journal homepage: www.elsevier.com/locate/anucene

Understanding the neutron noise induced by fuel assembly vibrations in linear theory

C. Demazière [a,*], A. Rouchon [b], A. Zoia [b]

[a] Chalmers University of Technology, Department of Physics, Division of Subatomic, High Energy and Plasma Physics, SE-412 96 Gothenburg, Sweden
[b] Université Paris-Saclay, CEA, Service d'études des réacteurs et de mathématiques appliquées, 91191 Gif-sur-Yvette, France

ARTICLE INFO

Article history:
Received 22 March 2022
Received in revised form 19 April 2022
Accepted 23 April 2022

ABSTRACT

This paper investigates the underlying physical mechanisms involved in the monochromatic vibrations of fuel assemblies and their effects on the induced neutron noise throughout the core of nuclear reactors, in the framework of simplified benchmark configurations. Any vibrating fuel pin introduces noise sources at the frequency of vibrations, as well as at higher harmonics, the first one being the most significant of those. Depending on the harmonics considered, the position of the vibrating fuel pin, the size of the core and its macroscopic cross-sections, different noise responses are observed within the reactor core. Through the lens of a decomposition of the neutron noise into its point-kinetics component and its deviation from it, the spectrum of noise responses is explained and related to the spatial distribution of the amplitude and phase of the noise sources at the considered frequencies. At the frequency of vibration, possible out-of-phase behaviour of the induced neutron noise can be partially or totally shadowed by the in-phase point-kinetics component, the only exception being for central vibrations in symmetrical systems. At the frequency of the first higher harmonics, the structure of the induced neutron noise is more involved. Nevertheless, due to the compensation of the individual responses associated to the different components of the noise source at that frequency, point-kinetics has a significant contribution. The results of this work sheds new light on the complex spatial pattern of the neutron noise computed by realistic core simulators in case of vibrations of fuel assemblies.

1. Introduction

Neutron noise, defined as the deviation of the instantaneous neutron flux from its mean value in time, assuming stationary conditions, provides some meaningful information about the state of a nuclear reactor (Thie, 1981; Pázsit and Demazière, 2010). In recent years, neutron noise analysis received renewed interest, especially following an apparent generic increase of the neutron noise observed in some of the Kraftwerk Union (KWU) type Pressurized Water Reactors (PWRs) – see, e.g., (Seidl et al., 2015). Although still not confirmed, this increase seems to be attributed to several noise sources co-existing at the same time in the system, one of which corresponds to the vibrations of fuel assemblies, either individually or collectively (Durrant et al., 2021; Viebach et al., 2019).

In order to support this hypothesis, calculations of the neutron noise were undertaken, and various advanced neutron noise modelling capabilities were developed as part of the European Horizon 2020 CORTEX project (CORe monitoring Techniques and EXperimental validation and demonstration) (Demazière et al., 2018; Vidal-Ferràndiz et al., 2020a, 2020b and 2020c; Vinai et al., 2021a). The modelling capabilities consider different refinements in the spatial, angular and energy, respectively, distribution of the neutron flux, using either time-domain or frequency-domain approaches, relying either on deterministic or probabilistic (i.e., Monte Carlo) methods, and assuming either a linear or non-linear approximation of the governing equations.

Due to the novel character of the neutron noise modelling tools thus developed, an extensive program of code validation was carried out in CORTEX (Lamirand et al., 2020; Vinai et al., 2021b). Dedicated neutron noise experiments were performed at two research reactors: the CROCUS reactor at the Ecole Polytechnique Fédérale de Lausanne, Lausanne, Switzerland, and the AKR-2 reactor at the Technical University of Dresden, Dresden, Germany.

Three experimental campaigns were undertaken at each facility. At AKR-2, two types of perturbations were considered: either by rotating a neutron absorbing foil along a horizontal axis or by moving a neutron absorbing disc along a horizontal axis. The former corresponds to a vibrating absorber, whereas the latter corresponds to an absorber of variable strength. At CROCUS, two perturbing devices were implemented: the COLIBRI device and

* Corresponding author.
E-mail addresses: demaz@chalmers.se (C. Demazière), amelie.rouchon@cea.fr (A. Rouchon), andrea.zoia@cea.fr (A. Zoia).

https://doi.org/10.1016/j.anucene.2022.109169
0306-4549/

the POLLEN vibrating absorber. In COLIBRI, up to 18 fuel rods located at the periphery of the core were laterally displaced with a sinusoidal forcing function. In POLLEN, a cadmium absorber located in a channel at the centre of the core was oscillating up and down.

In the case of vibrating absorbers, the spatial dependence of the amplitude and phase of the induced neutron noise at those two facilities was shown to be more complex than originally anticipated. This complexity was confirmed both in the measurement data themselves and in the corresponding computer simulations. Moreover, although the vibrations were supposed to occur at a single frequency, the actual displacement contained excitations at higher harmonics, as demonstrated for the case of COLIBRI in, e.g., (Brighenti et al., 2022). It should be noted that, even if the fuel assemblies were only vibrating at the fundamental angular frequency, higher harmonics in the response of the system would be observed, as earlier explained by Rouchon and Sanchez (2015) and Zoia et al. (2021) and as will be recalled in the following of this paper.

Likewise, when modelling fuel assembly vibrations in nuclear power reactors, the spatial dependence of the amplitude and phase of the induced neutron noise, both at the fundamental frequency and its first higher harmonics, was also demonstrated to exhibit different patterns, as demonstrated in, e.g., (Verma et al., 2021).

This paper is aimed at explaining the underlying principles leading to different spatial patterns of the neutron noise induced by fuel assembly vibrations, both at the fundamental frequency and its first higher harmonics. For this purpose, and in order to get physical understanding and insight, the system is kept as simple as possible. A benchmark configuration consisting in a three-region reactor is thus considered, with the inner region vibrating with respect to the two outer regions in a one-dimensional representation of the system. The induced neutron noise is estimated for different sizes of the system and for different equilibrium positions of the moving region. Using a decomposition of the neutron noise into a point-kinetics response and the deviation from it, the different spatial patterns are analysed. It will be demonstrated that various patterns of the induced neutron noise can indeed be explained using such a framework.

The paper is structured as follows. First, the representation of a moving region in terms of fluctuations of macroscopic cross-sections, which represent the input data of any simulation code, is detailed. Thereafter, the different systems considered for the analysis are presented, followed by a description of the modelling framework used for the analysis and its verification. The computed neutron noise is then analysed through the lens of projections onto its point-kinetics component and its deviation from it. The paper ends with highlighting the main conclusions of the work, with the aim to provide guidance to reactor physics experts analysists for the interpretation of the measured or calculated neutron noise.

2. Modelling of the noise source in case of fuel assembly vibrations

Due to mostly turbulence in the case of Pressurized Water Reactors and boiling in the case of Boiling Water Reactors, fuel assembly vibrate. Different types of oscillations are typically encountered (Bläsius, 2018; Demazière and Dokhane, 2019), as summarized in Table 1. This table gives the axial shape of the shape of the maximum displacement of a vibrating fuel assembly $d(z/H)$, together with the typical oscillation frequency ω_0. Here, z represents the considered core elevation and H the total core height. The instantaneous displacement at a given core elevation, denoted $\varepsilon(z,t)$, is thus proportional to:

$$\varepsilon(z,t) \propto d(z/H)\cos(\omega_0 t + \varphi) \tag{1}$$

where φ represents a possible phase shift or time delay. As seen in the Table, the main differences between the various types and modes of vibrations lie in the axial dependence of the movement of the fuel assembly. It should be noted that the illustrations in the Table represent the possible spatial modes of the axial displacement d(z/H). Such modes should not be confused with the harmonics in the frequency spectrum of the neutron noise and noise source earlier mentioned, which we will return to in the following of this paper.

Table 1
Main types of fuel assembly vibrations typically observed in commercial light water reactors.

Vibration modes	Cantilevered beam	Simply supported on both sides	Cantilevered beam and simply supported
Axial shape of the maximum displacement $d(z/H)$ in arbitrary units as a function of the relative core elevation z/H	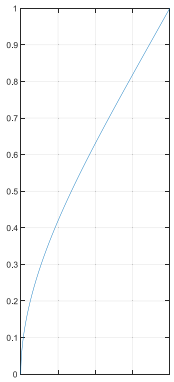	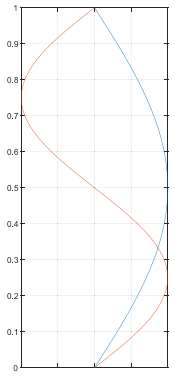 first axial mode in blue, second axial mode in orange	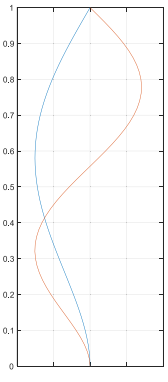 first axial mode in blue, second axial mode in orange
Oscillation frequency ω_0	Ca. 0.6 – 1.2 Hz	Ca. 0.8 – 4 Hz for the first axial mode Ca. 5 – 10 Hz for the second axial mode	Ca. 0.8 – 4 Hz for the first axial mode Ca. 5 – 10 Hz for the second axial mode

Disregarding the axial shape of the movement, fuel assembly vibrations along a given direction × can be seen as the collective displacement $\varepsilon(t)$ of the fuel pins belonging to that fuel assembly from their equilibrium positions, as conceptually represented in Fig. 1. From a neutronic viewpoint and neglecting the effect of burnup, the structures and their surroundings can be represented by sets of homogeneous regions, each having defined macroscopic cross-sections.

Vibrating structures can thus be seen as the displacement of the boundary between homogeneous regions. In order to better illustrate the modelling of such vibrations, two such adjacent regions are considered as depicted in Fig. 2 and are denoted as I and II in this figure. As the result of vibrations, the time-dependent boundary $b(t)$ is displaced by a distance $\varepsilon(t)$ from its equilibrium position b_0.

The various vibrating pins constituting a fuel assembly could then be represented by stacking several copies of the elementary model represented in Fig. 2. Furthermore, in a linear treatment of the neutron noise, as adopted in this work, the neutron noise induced by multiple noise sources is simply given by the superposition of the individual responses to each noise source. This thus justifies the emphasis on such an elementary lattice.

The spatial variation of any static macroscopic cross-section $\Sigma_{\alpha,0}$ of type α can thus be represented as (Jonsson et al., 2012):

$$\Sigma_{\alpha,0}(x) = [1 - \Theta(x - b_0)]\Sigma_{\alpha,I} + \Theta(x - b_0)\Sigma_{\alpha,II} \tag{2}$$

where Θ is the Heaviside function, and $\Sigma_{\alpha,I}$ and $\Sigma_{\alpha,II}$ represent the (static) macroscopic cross-section of type α for regions I and II, respectively. When the position of the boundary is perturbed as $b(t) = b_0 + \varepsilon(t)$, the deviation of the macroscopic cross-section of type α with respect to its static value is given as:

$$\delta\Sigma_\alpha(x,t) = \Delta\Sigma_\alpha\Theta(x - b_0 - \varepsilon(t)) - \Delta\Sigma_\alpha\Theta(x - b_0) \tag{3}$$

with $\Delta\Sigma_\alpha = \Sigma_{\alpha,II} - \Sigma_{\alpha,I}$. Assuming a sinusoidal displacement of the position of the boundary from its equilibrium position as $\varepsilon(t) = d\sin(\omega_0 t)$, adopting the model of Rouchon and Sanchez (2015), one could demonstrate that the Fourier transform of the perturbation of the macroscopic cross-section Σ_α, defined as:

$$\delta\Sigma_\alpha(x,\omega) = \int_{-\infty}^{+\infty} \delta\Sigma_\alpha(x,t)\exp(-i\omega t)dt \tag{4}$$

results in:

- If $x \in [b_0 - d; b_0 + d]$:

$$\begin{aligned}
&\delta\Sigma_\alpha(x,\omega) \\
&= -\text{sign}[\tau(x)] \times \Delta\Sigma_\alpha \times [\pi - 2\omega_0|\tau(x)|] \times \delta(\omega) \\
&+ \sum_{k=-\infty}^{+\infty} \frac{2i\Delta\Sigma_\alpha}{2k+1}\cos[(2k+1)\omega_0\tau(x)] \times \delta[\omega - (2k+1)\omega_0] \\
&+ \sum_{\substack{k=-\infty \\ k\neq 0}}^{+\infty} \frac{2\Delta\Sigma_\alpha}{2k}\sin[2k\omega_0\tau(x)] \times \delta[\omega - 2k\omega_0]
\end{aligned} \tag{5}$$

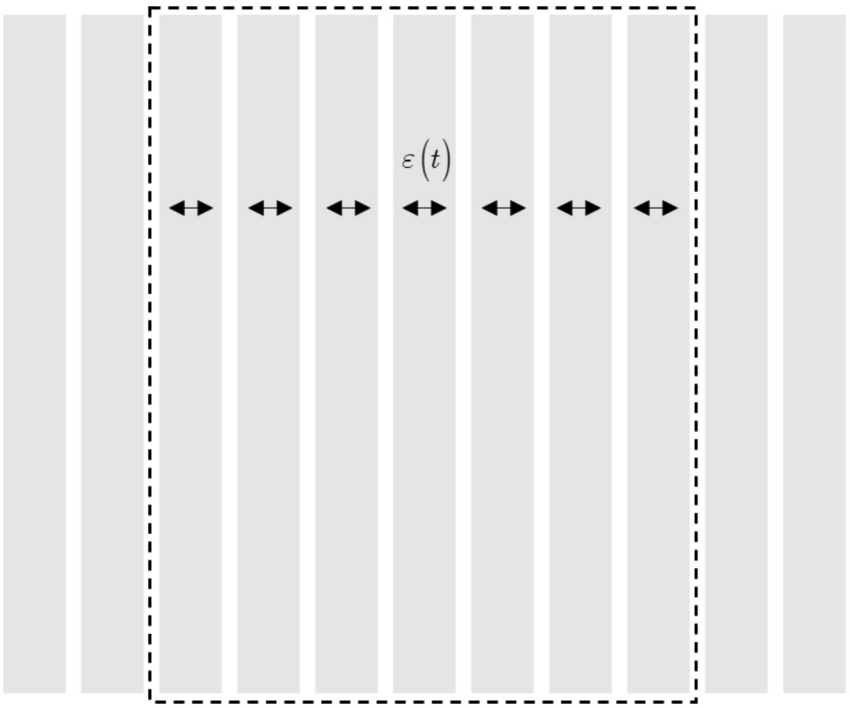

Fig. 1. Conceptual illustration of the lateral displacement of the pins in a vibrating fuel assembly.

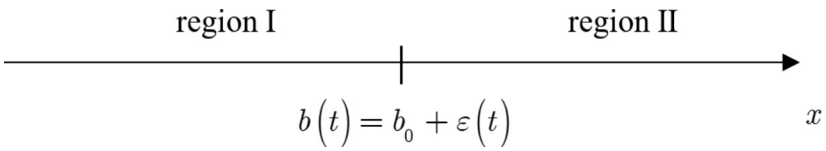

Fig. 2. Elementary one-dimensional lattice representing two homogeneous regions and their time-dependent boundary.

- If $x \notin [b_0 - d; b_0 + d]$:

$$\delta\Sigma_\alpha(x,\omega) = 0 \tag{6}$$

with.

$$\tau(x) = \frac{1}{\omega_0}\arcsin\left(\frac{x-b_0}{d}\right) \tag{7}$$

One notices from the above that, in addition to a perturbation at the fundamental angular frequency ω_0, the movement of the boundary also creates perturbations at higher harmonics $n\omega_0$, with n being an integer strictly larger than unity.

As will be illustrated in the following of this paper, turning to the frequency-domain allows a direct resolution of the induced neutron noise. A frequency-domain approach is thus adopted in the remaining of this paper.

Simpler representations of vibrating structures are also available in the literature, such as the so-called ε/d model (Pázsit and Karlsson, 1997). This model can be considered as a first-order approximation of the model given by Eqs. (4)-(6) for the fundamental angular frequency ω_0. At that angular frequency, the induced neutron noise was demonstrated to be in very good agreement between those two noise source models (Vidal-Ferrándiz et al., 2020a, 2020b; Zoia et al., 2021).

3. Description of the test systems

The neutron noise induced by fuel assembly vibrations is considered hereafter for two systems: a small reactor of 1 m in size and a large reactor of 3 m in size. Both systems are light water reactor cores. The small system could be considered as representative of, e.g., the CROCUS reactor, whereas the large system is representative of a commercial LWR. The problem is kept as simple as possible, i.e., a three-region system is modelled, where the inner region is 1 cm wide and is vibrating. The boundaries between adjacent regions are moving according to the model presented in Section 2 in order to mimic the effect of vibrating structures, with $d = 0.5$ cm and $\omega_0/2\pi = 1$ Hz. The system can thus be considered as representative of a fuel pin vibrating in two neighbouring homogeneous regions.

The simplicity of the model allows shedding light on the physics of vibrating structures. Moreover, the governing equations can also be solved analytically, which will be used in the following of this paper to demonstrate the correctness of the numerical solution. One-group diffusion theory and one family of delayed neutrons are used in this work. The corresponding macroscopic cross-sections and kinetics parameters are given in Table 2.

4. Description and verification of the modelling framework

In this work, the calculations of the neutron noise are performed in the frequency domain, without any thermal–hydraulic feedback, in linear theory (i.e., neglecting second-order terms in the fluctuating quantities) and for a one-dimensional representation of the systems.

It was earlier demonstrated that, even for pin modelling, diffusion theory gives reasonable results as compared to transport theory, as long as a sufficient fine mesh is used (Vinai et al., 2021c). The calculations hereafter reported are thus based on a fine mesh, also required by the fact that the spatial regions on which the perturbations are defined are small. Although differences with transport exist, the purpose of this work is to understand different trends in system responses, for which diffusion theory is sufficient.

The calculations are carried out using a modified version of the CORE SIM tool (Demazière, 2011). The modifications primarily concern the number of energy groups (one energy group instead of two originally), the use of zero flux boundary conditions (instead of Marshak boundary conditions) and the number of spatial dimensions considered (one dimension instead of three originally). The reduction in the spatial dimensionality, thanks to the corresponding reduction in computer memory, allows making use of superfine mesh in the selected direction. A mesh size of 0.01 cm was used throughout this work.

Moreover, using one-group diffusion theory makes it possible to solve the problem analytically, which can be used to verify the correctness of the CORE SIM numerical solution for modelling vibrating structures.

A recent analysis of the applicability of linear theory for neutron noise calculations highlighted the necessity in some specific situations to include the effect of higher-order terms when considering vibrating fuel pins (Zoia et al., 2021). In transport theory, higher-order terms were demonstrated to play a non-negligible role when estimating the impact of the different harmonics on each other. Most notably, for the case of central perturbations in very small systems and in linear theory, the amplitude of the second harmonics at $2\omega_0$ in the induced neutron noise was found to be much larger than the amplitude of the first harmonics at ω_0. Nevertheless, when including non-linear terms in the modelling, the amplitude of the second harmonics was greatly reduced. Such an unphysical "explosion" of the second harmonics in linear theory was also attributed to steep gradients of the static neutron flux in the neighbourhood of the applied perturbations. In the analysis reported hereafter, the conditions leading to an unphysical "explosion" of the second harmonics as compared to the first harmonics are not met, and it is thus acceptable to use a linear treatment of the balance equations at both the fundamental frequency and its first higher harmonics.

The systems considered in this analysis are defined on the spatial domain $x \in [-a; a]$, with $2a$ being the system size (either $2a = 1$ m for the small system or $2a = 3$ m for the large system). The reactors are made of three consecutive regions labelled I, II and III, respectively, with b and c representing the position of the corresponding interfaces. Region II represents the moving structure. Various equilibrium positions of Region II are considered hereafter. Nevertheless, the width of this region is fixed at 1 cm, i.e., $c - b = 1$ cm.

Before turning to the analysis of the results for different system sizes and different equilibrium positions of the moving region, the analytical solution to the problem is first derived, so that the correctness of the CORE SIM solution can be demonstrated. Although the primary interest of this work lies on the neutron noise, the analytical expressions for both the static flux and the neutron noise are first given, as the static neutron flux and the corresponding eigenvalue are required for the estimation of the neutron noise.

The static solution is given by:

$$\phi_0(x) = \begin{cases} A_I \sin\left[B_{m,I}(x+a)\right] \text{ for } x \le b \\ A_{II}^{+}\exp\left[iB_{m,II}x\right] + A_{II}^{-}\exp\left[-iB_{m,II}x\right] \text{ for } b \le x \le c \\ A_{III}\sin\left[B_{m,III}(x-a)\right] \text{ for } c \le x \end{cases} \tag{8}$$

where the material buckling in any of the regions labelled N is defined as:

$$B_{m,N}^2 = \frac{\nu\Sigma_{f,0,N}/k_{eff} - \Sigma_{a,0,N}}{D_{0,N}} \tag{9}$$

The criticality condition is obtained as follows. The continuity of the static neutron flux and the neutron net current, respectively, expressed in both $x = b$ and $x = c$, gives a set of four homogeneous algebraic equations for the amplitude coefficients A_I, A_{II}^{+}, A_{II}^{-} and A_{III}. The only possibility for having non-zero solutions for the amplitude coefficients is to force the determinant corresponding to this

Table 2
Macroscopic cross-section data and kinetics parameters used in the small and large reactor models.

	Small system of 1 m in size		Large system of 3 m in size	
	Inner region	Outer regions	Inner region	Outer regions
Diffusion coefficient, D_0 [cm]	1.3410	1.3410	1.3410	1.3410
Macroscopic absorption cross-section, $\Sigma_{a,0}$ [cm^{-1}]	1.8983x10^{-2}	2.0881x10^{-2}	1.7825x10^{-2}	1.9608x10^{-2}
Macroscopic fission cross-section times the average number of neutrons emitted per fission event, $\nu\Sigma_{f,0}$ [cm^{-1}]	2.3300x10^{-2}	2.0970x10^{-2}	2.3300x10^{-2}	2.0970x10^{-2}
Average neutron velocity, υ [cm.s^{-1}]	2.2x10^5			
Fraction of delayed neutrons, β [pcm]	600			
Decay constant of the precursors of delayed neutrons, λ [s^{-1}]	0.08			

system of equations to be equal to zero. This is achieved by adjusting k_{eff}, from which the criticality of the system is determined. The criticality search is performed numerically in this work.

The neutron noise in the frequency-domain can then be estimated as (Pázsit and Demazière, 2010):

$$\delta\phi(x,\omega) = \int G(x,x',\omega)\delta S(x',\omega)\phi_0(x')dx' \tag{10}$$

where the Green's function $G(x,x',\omega)$ is expressed as:

- If $x' \leq b$:

$$G(x,x',\omega) = \begin{cases} C_I \sin\left[B_I(\omega)(x+a)\right] \text{ for } x \leq x' \\ D_I \exp\left[iB_I(\omega)x\right] + E_I \exp\left[-iB_I(\omega)x\right] \text{ for } x' \leq x \leq b \\ F_{II} \exp\left[iB_{II}(\omega)x\right] + G_{II}\exp\left[-iB_{II}(\omega)x\right] \text{ for } b \leq x \leq c \\ H_{III} \sin\left[B_{III}(\omega)(x-a)\right] \text{ for } c \leq x \end{cases} \tag{11}$$

- If $b \leq x' \leq c$:

$$G(x,x',\omega) = \begin{cases} C_I \sin\left[B_I(\omega)(x+a)\right] \text{ for } x \leq b \\ D_{II} \exp\left[iB_{II}(\omega)x\right] + E_{II} \exp\left[-iB_{II}(\omega)x\right] \text{ for } b \leq x \leq x' \\ F_{II} \exp\left[iB_{II}(\omega)x\right] + G_{II} \exp\left[-iB_{II}(\omega)x\right] \text{ for } x' \leq x \leq c \\ H_{III} \sin\left[B_{III}(\omega)(x-a)\right] \text{ for } c \leq x \end{cases} \tag{12}$$

- If $x' \geq c$:

$$G(x,x',\omega) = \begin{cases} C_I \sin\left[B_I(\omega)(x+a)\right] \text{for } x \leq b \\ D_{II} \exp\left[iB_{II}(\omega)x\right] + E_{II} \exp\left[-iB_{II}(\omega)x\right] \text{for } b \leq x \leq c \\ F_{III} \exp\left[iB_{III}(\omega)x\right] + G_{III} \exp\left[-iB_{III}(\omega)x\right] \text{for } c \leq x \leq x' \\ H_{III} \sin\left[B_{III}(\omega)(x-a)\right] \text{for } x' \leq x \end{cases} \tag{13}$$

The "dynamic" buckling in any of the regions labelled N is defined as:

$$B_N^2(\omega) = \frac{\left(1 - \frac{i\omega\beta}{i\omega+\lambda}\right)\frac{\upsilon\Sigma_{f,0,N}}{k_{eff}} - \Sigma_{a,0,N} - \frac{i\omega}{\upsilon}}{D_{0,N}} \tag{14}$$

The amplitude coefficients C_I, $D_{I/II}$, $E_{I/II}$, $F_{II/III}$, $G_{II/III}$ and H_{III} are obtained by expressing:

- The continuity of the Green's function at the noise source location x' and in b and c.
- The continuity of the gradient of the Green's function in b and c, and the discontinuity of the gradient of the Green's function at the noise source location x'.

In Eq. (10), the cross-section perturbations $\delta S(x,\omega)$ are expressed as:

$$\delta S(x,\omega) = \delta\Sigma_a(x,\omega) - \left(1 - \frac{i\omega\beta}{i\omega+\lambda}\right)\frac{\delta\upsilon\Sigma_f(x,\omega)}{k_{eff}} \tag{15}$$

with the perturbations of the macroscopic cross-sections $\delta\Sigma_a(x,\omega)$ and $\delta\upsilon\Sigma_f(x,\omega)$ given by Eqs. (8)-(14) applied to each of the boundaries located at b and c. In the following of this paper, the noise source is defined from Eq. (15) as $\delta S(x,\omega)\phi_0(x)$.

The integration of Eq. (10) is performed numerically. The neutron noise estimated using Eqs. (8)-(14), despite relying on analytical expressions, will be referred to in the following as a semi-analytical solution, as both the integration of Eq. (10) and the criticality search are performed numerically. Such a semi-analytical solution is considered as the reference solution, used hereafter to verify the correctness of the CORE SIM solution.

Before turning to the induced neutron noise $\delta\phi(x,\omega)$, the noise source $\delta S(x,\omega)\phi_0(x)$ corresponding to an inner moving region is examined. In the frequency domain, the spatial dependence of the amplitude and phase of the noise source $\delta S(x,\omega)\phi_0(x)$, with δS defined in Eq. (15), is represented in Fig. 3 for the large reactor system with the set of cross-sections defined in Table 2, both at the fundamental frequency of $\omega_0/2\pi = 1$ Hz and at the $2\omega_0/2\pi = 2$ Hz harmonics. At the fundamental frequency, the noise source is given by two contributions related to each of the two moving boundaries located in b and c, respectively. With respect to each moving boundary, the contributions are symmetrical, i.e., they have the same phase. With respect to the centre of the moving region, the contributions are anti-symmetrical, i.e., they are out-of-phase. For the first higher harmonics, on the other hand, each of the contributions is anti-symmetrical with respect to its moving boundary. Nevertheless, with respect to the centre of the moving region, the two contributions are symmetrical.

The comparison between the CORE SIM simulations and the semi-analytical (reference) solution obtained by Eq. (10) is represented for $b = -35.5$ cm and $c = -34.5$ cm in Figs. 4 and 5, giving the spatial dependence of the solution throughout the entire system and around the perturbed boundaries, respectively, for the large system. Comparisons are carried out at both the fundamental frequency of $\omega_0/2\pi = 1$ Hz and at the $2\omega_0/2\pi = 2$ Hz harmonics. As seen in those figures, the agreement between the CORE SIM and semi-analytical solutions is excellent, both regarding the amplitude and phase of the induced neutron noise. This demonstrates the capability of CORE SIM to correctly estimate the neutron noise for closely located moving boundaries.

5. Results

Based on the successful verification of the CORE SIM tool to model vibrating structures, a systematic analysis of the induced neutron noise was undertaken, using solely CORE SIM. The different conditions investigated in this work are summarized below:

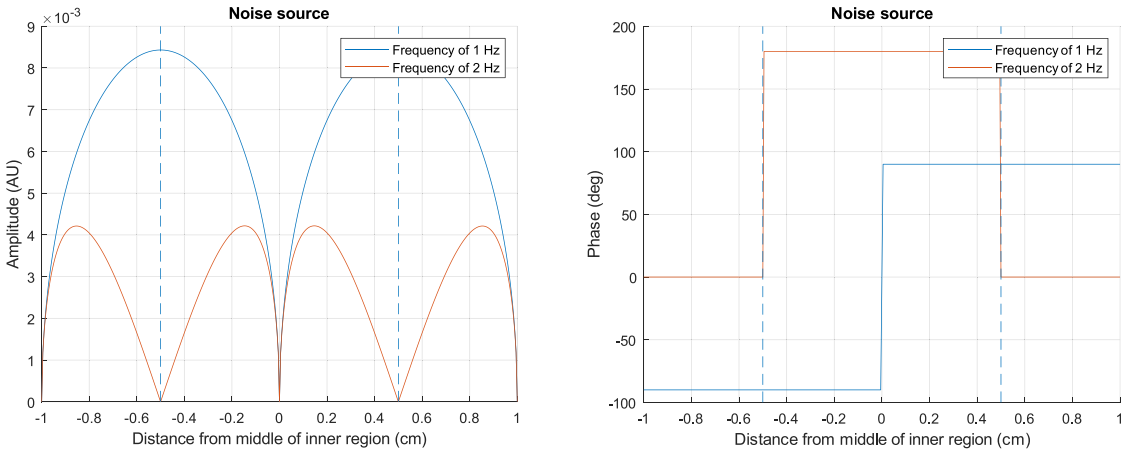

Fig. 3. Amplitude (left figure) and phase (right figure) of the noise source $\delta S(x,\omega)\phi_0(x)$ at 1 Hz and 2 Hz in the case of an inner region moving relative to two outer regions in the large reactor system. The plots correspond to the case of a centrally located innermost region (the plots are nevertheless identical to the naked eye for an off-centred innermost region).

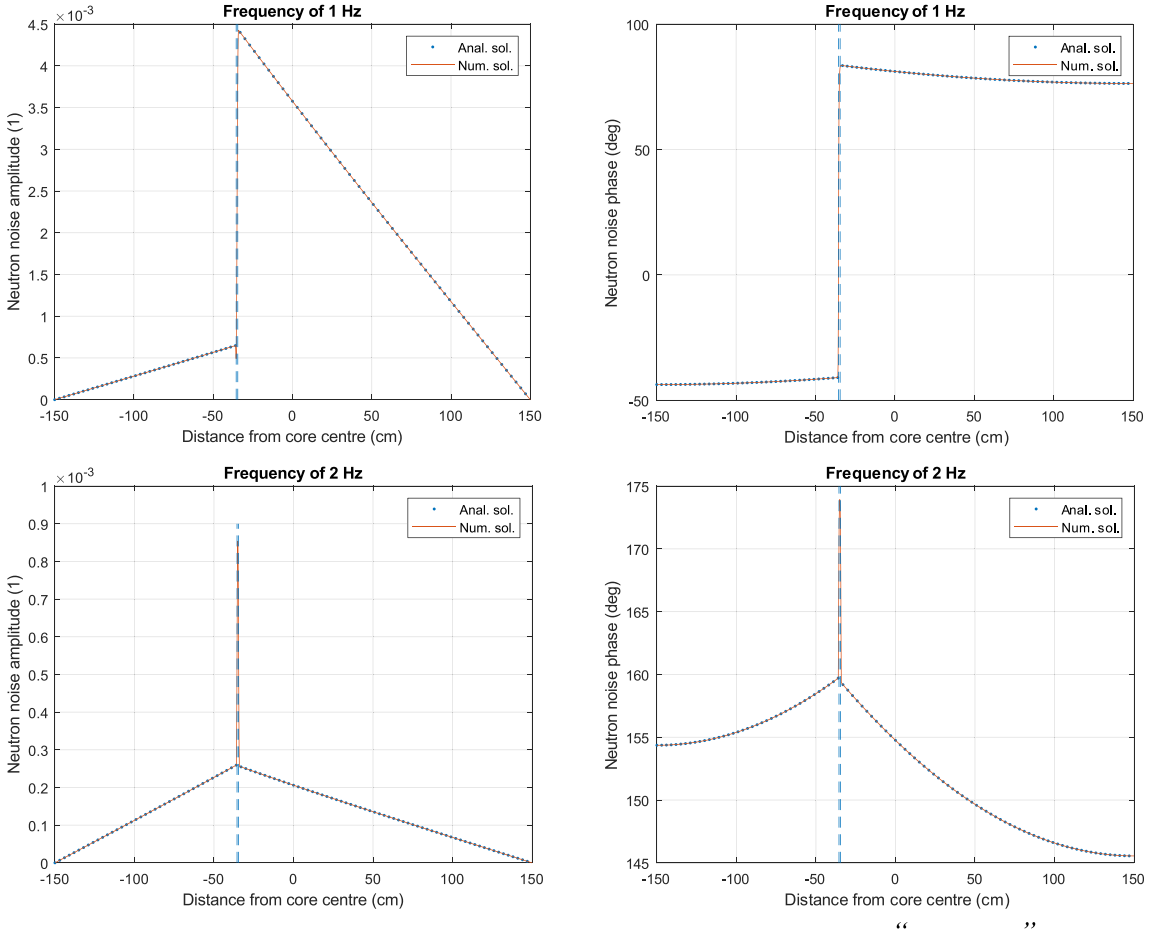

Fig. 4. Comparisons between the results of the CORE SIM solution (labelled "Num. sol.") and the semi-analytical solution (labelled "Anal. sol.") for the large reactor system and for an inner moving region located at equilibrium between $b = -35.5$ cm and $c = -34.5$ cm. The amplitude of the induced neutron noise is given on the left figures and its phase on the right figures, whereas the results at 1 Hz are given in the top figures and the ones at 2 Hz are given in the bottom figures.

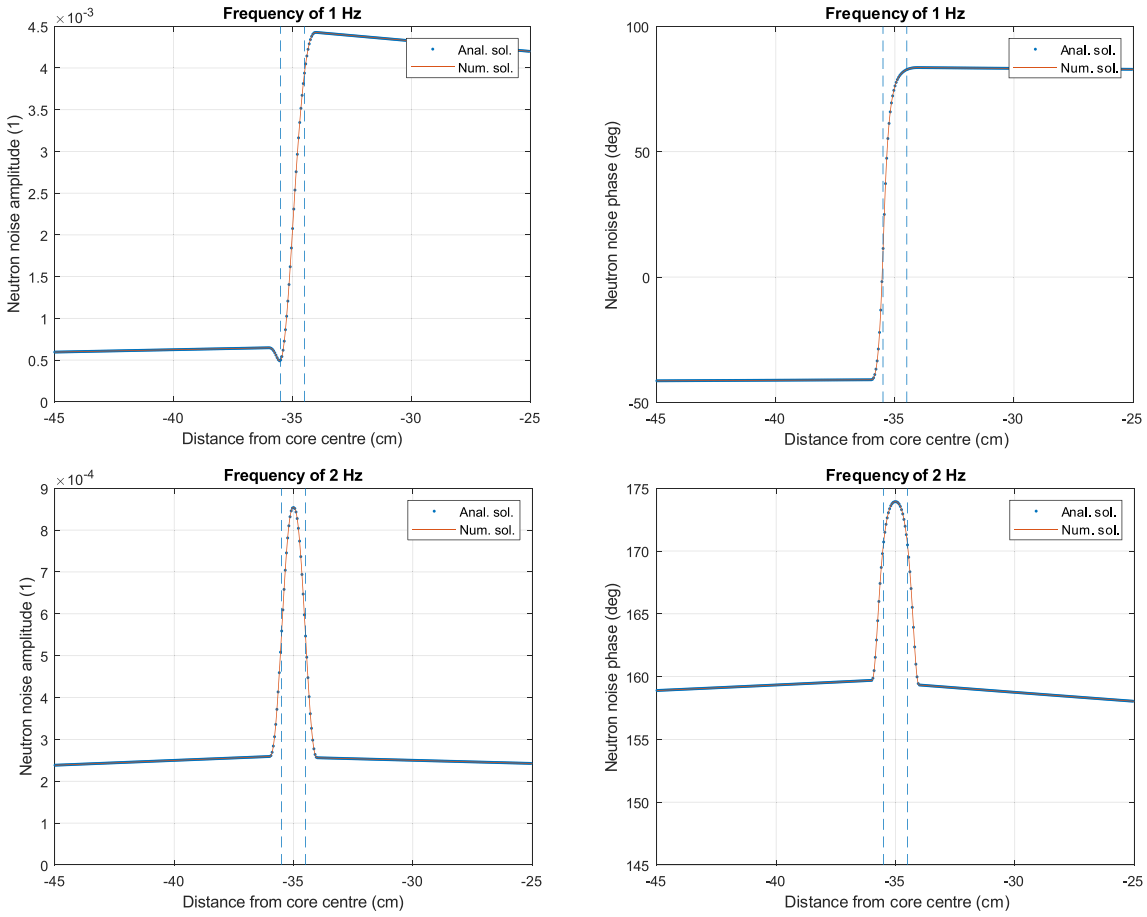

Fig. 5. Comparisons between the results of the CORE SIM solution (labelled "Num. sol.") and the semi-analytical solution (labelled "Anal. sol.") in the close vicinity of the moving boundaries for the large reactor system and for an inner moving region located at equilibrium between $b = -35.5$ cm and $c = -34.5$ cm. The amplitude of the induced neutron noise is given on the left figures and its phase on the right figures, whereas the results at 1 Hz are given in the top figures and the ones at 2 Hz are given in the bottom figures.

- Two system sizes were considered: a large system of size $2a = 3$ m and a small system of size $2a = 1$ m.
- For each system, three equilibrium positions of the inner vibrating region were considered:
  - o A central perturbation, for which the centre of the moving region at equilibrium is defined as $(b + c)/2 = 0$ cm.
  - o A mid-core perturbation, for which the centre of the moving region at equilibrium is defined as $(b + c)/2 = -a/3$.
  - o A peripheral perturbation, for which the centre of the moving region at equilibrium is defined as $(b + c)/2 = -2a/3$.
- For each system size and equilibrium position of the inner vibrating region, both the neutron noise induced at the fundamental frequency of $\omega_0/2\pi = 1$ Hz and its first higher harmonics at $2\omega_0/2\pi = 2$ Hz were estimated.

For all the cases listed above, the induced neutron noise was also decomposed into the neutron noise components induced by each of the two moving boundaries, respectively. The neutron noise induced by the vibration of the boundary having for equilibrium position b only was estimated separately (referred to as "left-induced only neutron noise"). Likewise, the neutron noise induced by the vibration of the boundary having for equilibrium position c only was estimated separately (referred to as "right-induced only neutron noise").

6. Analysis framework

In order to get a better physical understanding, the neutron noise is decomposed into its point-kinetics component and the remaining component, as explained hereafter. First, the time- and space-dependent neutron flux $\phi(x, t)$ is factorized into an amplitude factor $P(t)$ and a shape function $\psi(x, t)$ as (Bell and Glasstone, 1970):

$$\phi(x, t) = P(t)\psi(x, t) \tag{16}$$

where the amplitude factor is only time-dependent, whereas the shape function is both space- and time-dependent. If one chooses the following normalization condition for the shape function:

$$\frac{\partial}{\partial t}\int_R \phi_0(x)\psi(x, t)dx = 0 \tag{17}$$

where R represents the domain of integration over the entire system, the amplitude factor is solution of the point-kinetics equations, which are not recalled here for the sake of brevity. We refer instead to, e.g., (Bell and Glasstone, 1970).

Splitting the amplitude factor and shape function into a mean (i.e., steady-state) value and a fluctuating part as:

$$P(t) = P_0 + \delta P(t) \tag{18}$$

and.

$$\psi(x,t) = \frac{\phi_0(x)}{P_0} + \delta\psi(x,t) \tag{19}$$

the neutron noise in the time-domain and in linear theory thus reads:

$$\delta\phi(x,t) \approx \phi_0(x)\frac{\delta P(t)}{P_0} + \delta\psi(x,t) \tag{20}$$

whereas, in the frequency-domain, one obtains:

$$\delta\phi(x,\omega) \approx \phi_0(x)\frac{\delta P(\omega)}{P_0} + \delta\psi(x,\omega) \tag{21}$$

The term $\phi_0(x)\delta P(\omega)/P_0$ is referred to as the point-kinetics component of the neutron noise, whereas the remaining component, $\delta\psi(x,\omega)$ corresponds to the fluctuations of the shape function. Moreover, it could be demonstrated that (Pázsit and Demazière, 2010):

$$\frac{\delta P(\omega)}{P_0} = G_0(\omega)\delta\rho(\omega) \tag{22}$$

where $G_0(\omega)$ is the so-called zero-power reactor transfer function and $\delta\rho(\omega)$ is the reactivity noise induced by the perturbation applied to the system. Using first-order perturbation theory, the reactivity noise is given in one-group theory, for the cross-section perturbations assumed in Eq. (15), as (Bell and Glasstone, 1970):

$$\delta\rho(\omega) = \frac{\int_R \left[\frac{\delta\upsilon\Sigma_f(x,\omega)}{k_{eff}} - \delta\Sigma_a(x,\omega)\right]\phi_0^2(x)dx}{\int_R \frac{\upsilon\Sigma_{f,0}(x)}{k_{eff}}\phi_0^2(x)dx} \tag{23}$$

Eq. (23) also highlights the fact that any perturbation spatially distributed such that:

$$\int_R \left[\frac{\delta\upsilon\Sigma_f(x,\omega)}{k_{eff}} - \delta\Sigma_a(x,\omega)\right]\phi_0^2(x)dx = 0 \tag{24}$$

leads to a zero-reactivity effect and, consequently, to the absence of any point-kinetics component in the reactor response.

As Eq. (21) demonstrates, the space-dependence of the point-kinetics component follows the one of the static flux, whereas the space-dependence of the fluctuations in the shape function can take any shape. As a consequence, there is no phase variation throughout the system related to the point-kinetics component. Any phase variation is entirely due to the one of the fluctuations of the shape function. Furthermore, as can be seen from Eq. (22), the strength of the point-kinetics component strongly depends on the strength of the reactivity noise, through the zero-power reactor transfer function. In other words, one can anticipate from Eq. (21) that a spatial response in the induced neutron noise can only differ from the one of the static flux if the point-kinetics component is not overwhelming. Depending on how important the point-kinetics component is, different spatial responses throughout the system will emerge. This is demonstrated in the following of this paper, where the induced neutron noise in the situations earlier identified is estimated, as well as its point-kinetics component and the deviation from it.

Although it would be possible to evaluate the point-kinetics component via Eq. (22) and subtract it from the induced neutron noise to get the fluctuations in the shape function, another approach was followed in this work. The initial condition $\phi(x,0) = \phi_0(x) = P_0\psi(x,0)$ leads, when using Eq. (17), to:

$$\int_R \phi_0(x)\delta\psi(x,t)dx = 0 \tag{25}$$

Consequently, one obtains, using Eq. (20):

$$\begin{aligned}\int_R \phi_0(x)\delta\phi(x,t)dx &= \frac{\delta P(t)}{P_0}\int_R \phi_0^2(x)dx + \int_R \phi_0(x)\delta\psi(x,t)dx \\ &= \frac{\delta P(t)}{P_0}\int_R \phi_0^2(x)dx\end{aligned} \tag{26}$$

from which it follows that:

$$\frac{\delta P(t)}{P_0} = \frac{\int_R \phi_0(x)\delta\phi(x,t)dx}{\int_R \phi_0^2(x)dx} \tag{27}$$

or, in the frequency-domain:

$$\frac{\delta P(\omega)}{P_0} = \frac{\int_R \phi_0(x)\delta\phi(x,\omega)dx}{\int_R \phi_0^2(x)dx} \tag{28}$$

From the induced neutron noise$\delta\phi(x,\omega)$, $\delta P(\omega)/P_0$ can be estimated from Eq. (28). The point kinetics component of the induced neutron noise is then given by:

$$\delta\phi^{pk}(x,\omega) = \phi_0(x)\delta P(\omega)/P_0 \tag{29}$$

and the fluctuations of the shape function (also referred to as the deviation from point-kinetics) are thus given as:

$$\delta\psi(x,\omega) \approx \delta\phi(x,\omega) - \phi_0(x)\delta P(\omega)/P_0 \tag{30}$$

Compared to Eq. (22), this approach has the advantage of not requiring the computation of any extra quantity, such as the zero-power reactor transfer function and the reactivity noise.

In the following, the amplitude and phase of the neutron noise are given for the total neutron noise, for its point-kinetics component and for the fluctuations of the shape function.

Finally, since the calculations are all performed in linear theory, the neutron noise induced by multiple noise sources is equal to the sum of the neutron noise induced by each of the individual noise sources. In the present analysis, and in order to get deeper physical understanding, the neutron noise induced by the vibrating inner region was also decomposed into the neutron noise induced by the vibration of the boundary located at *b* and the neutron noise induced by the vibration of the boundary located at *c*.

7. Analysis of the neutron noise at the fundamental frequency

The amplitude and phase of the neutron noise induced by the central perturbation are given in Figs. 6 and 7, respectively. The amplitude and phase of the neutron noise induced by the mid-core perturbation are given in Figs. 8 and 9, respectively. The amplitude and phase of the neutron noise induced by the peripheral perturbation are given in Figs. 10 and 11, respectively. In all figures, the results of both the large and small systems are presented. Moreover, the neutron noise induced by the moving inner region is decomposed into the neutron noise induced by the vibration of the boundary located in *b* (referred to as "left-induced only neutron noise" in the figures) and the neutron noise induced by the vibration of the boundary located in *c* (referred to as "right-induced only neutron noise" in the figures).

As can be seen in Fig. 3 for the 1 Hz component, the noise source is represented by an anti-symmetrical (out-of-phase) perturbation around the centre of the moving region. Correspondingly, the induced neutron noise, being the result of the effect of the two noise sources being out-of-phase, stems from the respective neutron noise responses induced by each vibrating boundary being out-of-phase.

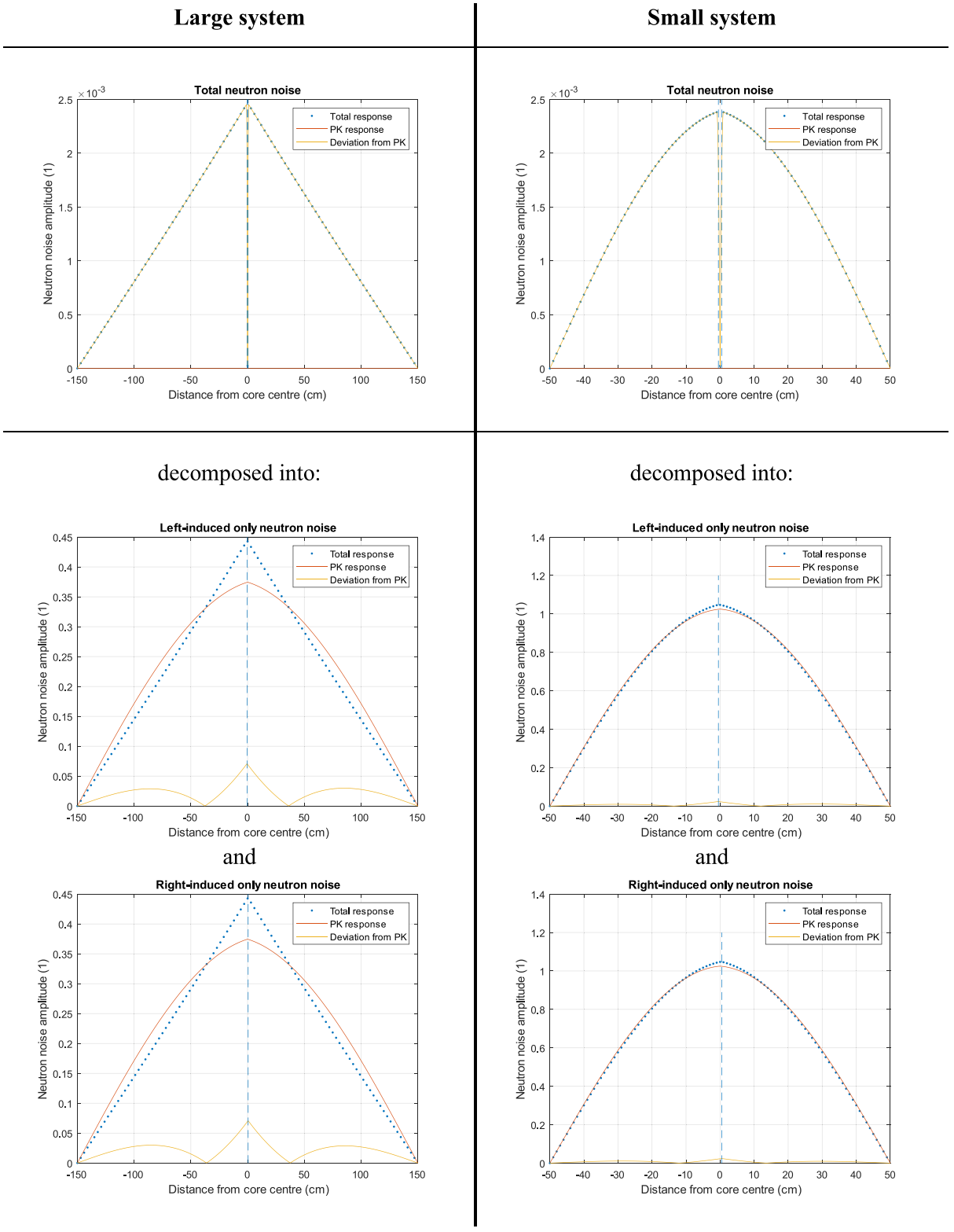

Fig. 6. Analysis of the amplitude of the neutron noise induced by a central perturbation at 1 Hz. The results for the large system are given on the left, whereas the results for the small system are given on the right. The top-row figures give the induced neutron noise, decomposed into the component induced by the vibration of the boundary located in *b* (mid-row figures) and into the component induced by the vibration of the boundary located in *c* (bottom-row figures). "PK" means point-kinetics.

7.1. Case of the central perturbation

Due to the symmetrical character of the two vibrating boundaries, the amplitude of the total neutron noise is several decades smaller than the neutron noise induced by each of the two vibrating boundaries.

Each of the two vibrating boundaries has a large point-kinetics contribution. As small systems behave essentially in a

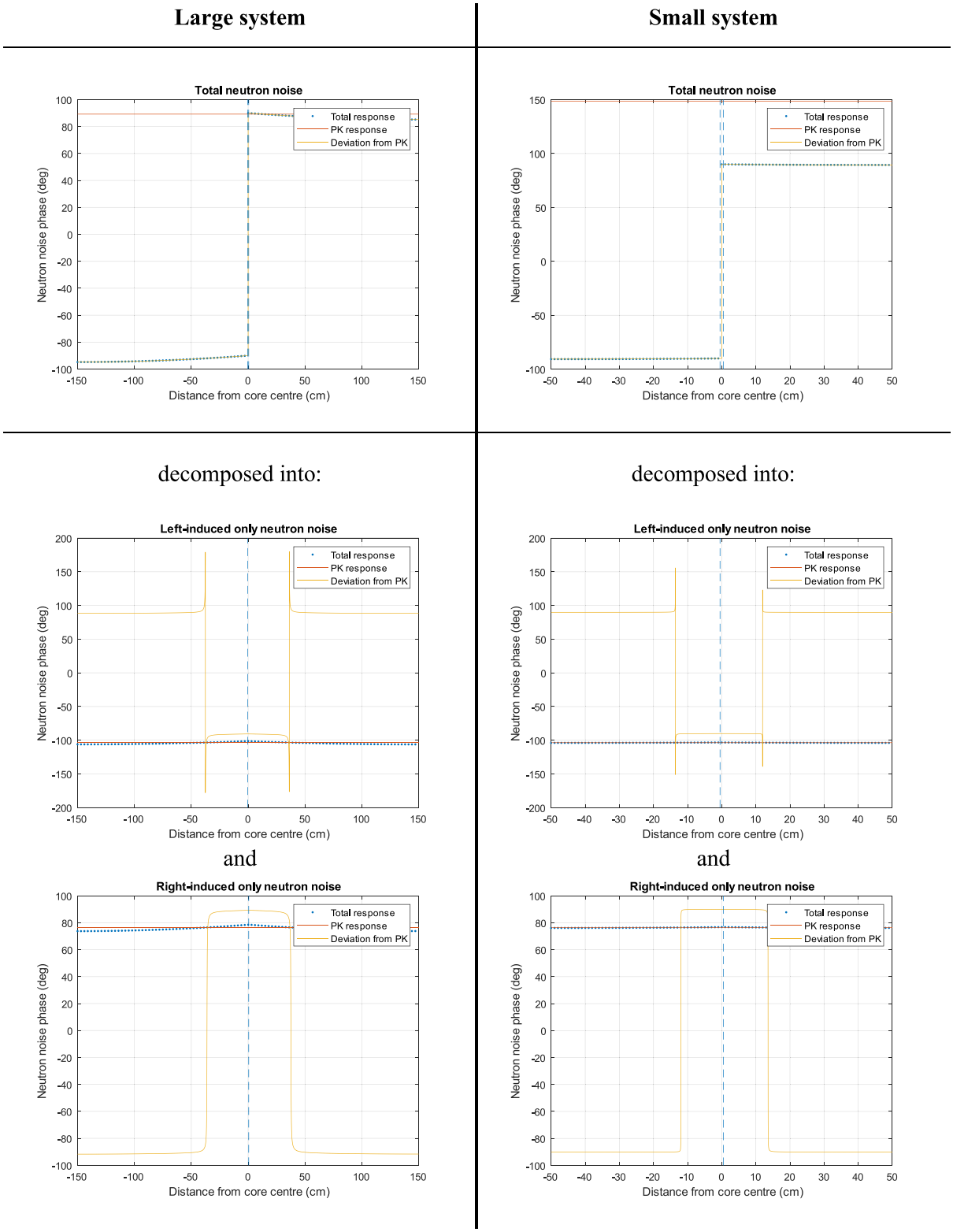

Fig. 7. Analysis of the phase of the neutron noise induced by a central perturbation at 1 Hz. The results for the large system are given on the left, whereas the results for the small system are given on the right. The top-row figures give the induced neutron noise, decomposed into the component induced by the vibration of the boundary located in *b* (mid-row figures) and into the component induced by the vibration of the boundary located in *c* (bottom-row figures). "PK" means point-kinetics.

point-kinetics manner (Pázsit and Demazière, 2010), the induced neutron noise corresponding to each vibrating boundary is entirely given by its point-kinetics contribution in the case of the small system.

Although the shape of the amplitude of the total noise resembles the one of the underlying point-kinetics contributions of the neutron noise induced by each of the two vibrating boundaries, one notices that the point-kinetics response is completely negligible. This is the result of the two noise sources being out-of-phase in an exactly symmetrical configuration. In other words, the total reactivity effect of the two noise sources is, due to the anti-symmetrical character of the noise sources, exactly zero – see Eq. (24).

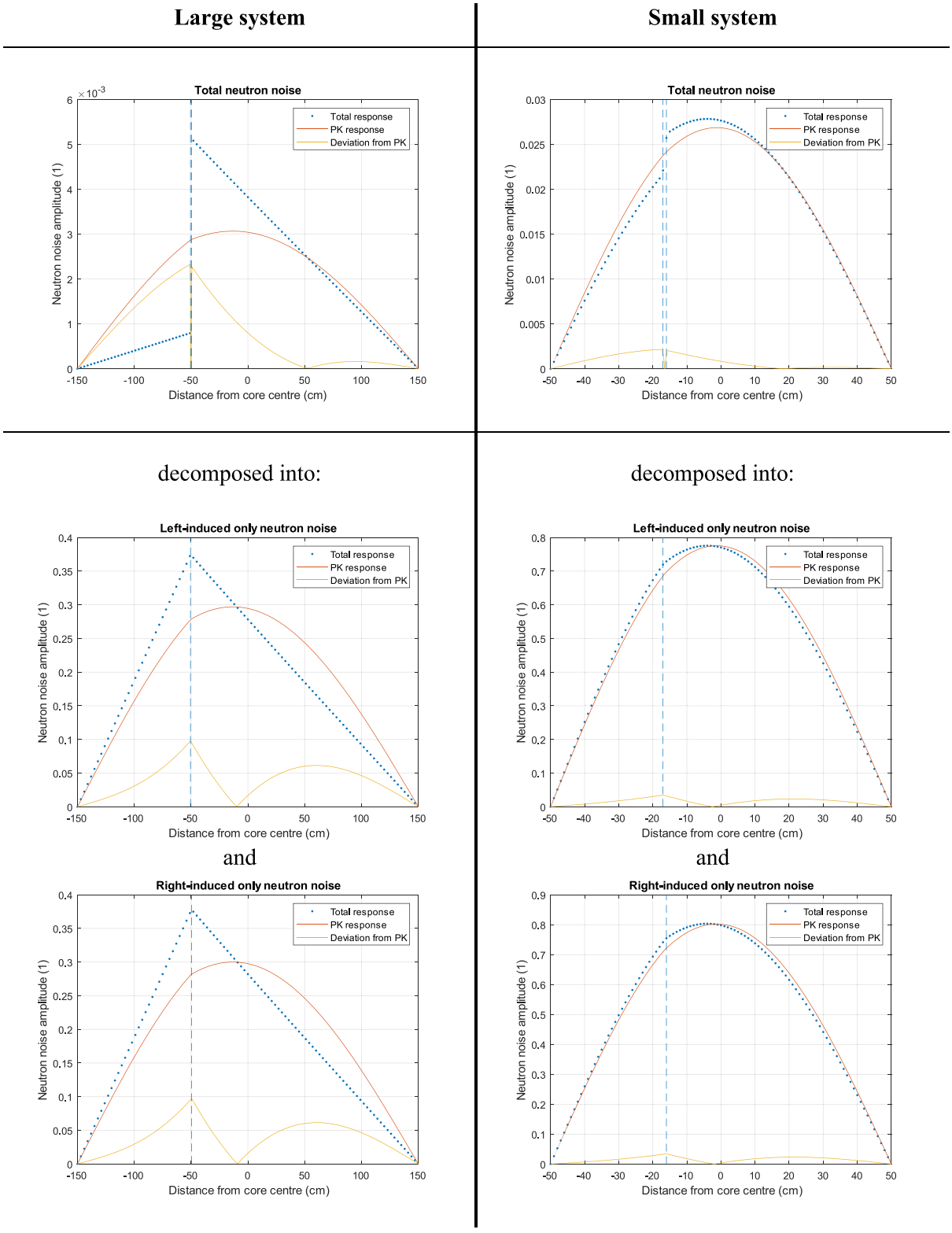

Fig. 8. Analysis of the amplitude of the neutron noise induced by a mid-core perturbation at 1 Hz. The results for the large system are given on the left, whereas the results for the small system are given on the right. The top-row figures give the induced neutron noise, decomposed into the component induced by the vibration of the boundary located in *b* (mid-row figures) and into the component induced by the vibration of the boundary located in *c* (bottom-row figures). "PK" means point-kinetics.

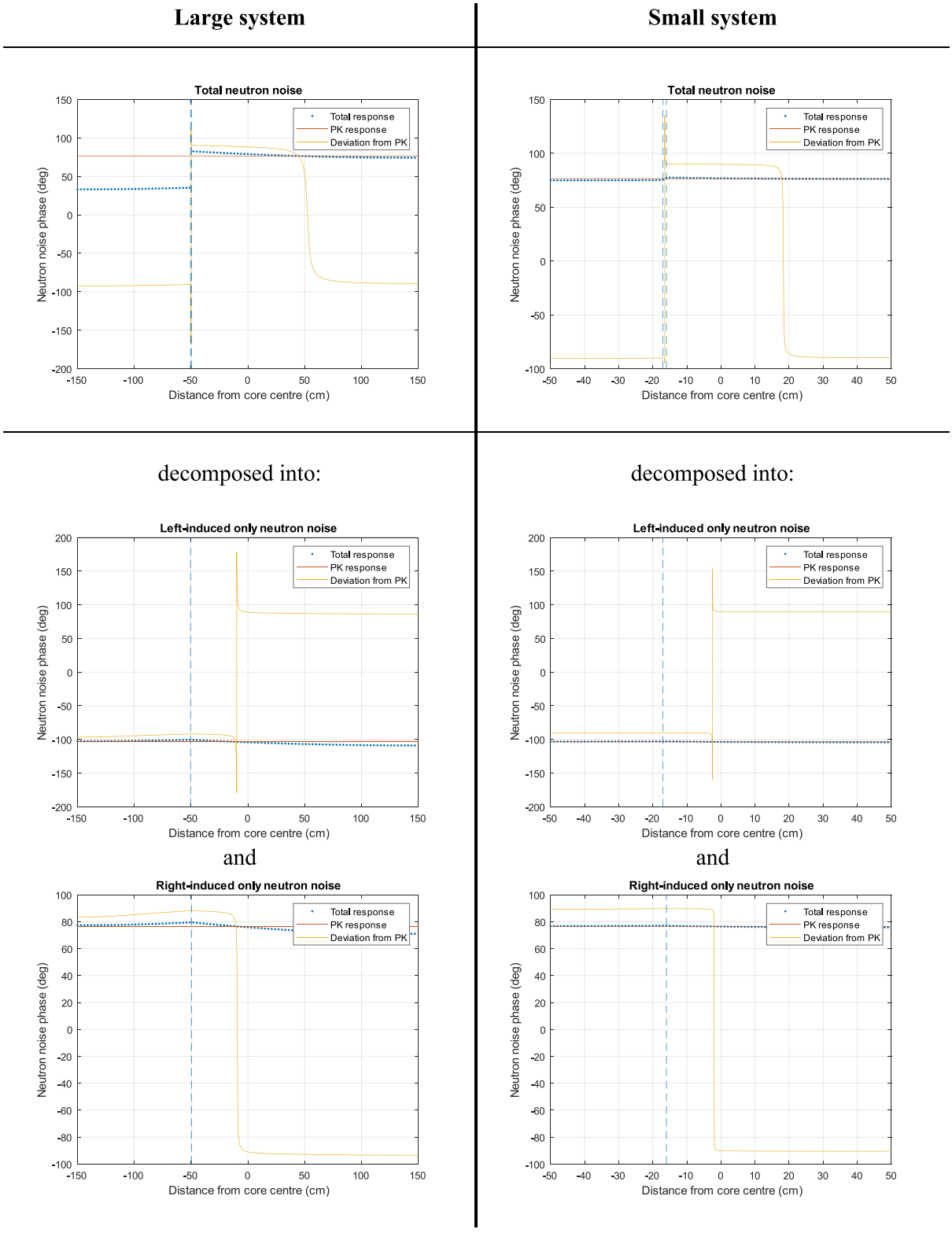

Fig. 9. Analysis of the phase of the neutron noise induced by a mid-core perturbation at 1 Hz. The results for the large system are given on the left, whereas the results for the small system are given on the right. The top-row figures give the induced neutron noise, decomposed into the component induced by the vibration of the boundary located in *b* (mid-row figures) and into the component induced by the vibration of the boundary located in *c* (bottom-row figures). "PK" means point-kinetics.

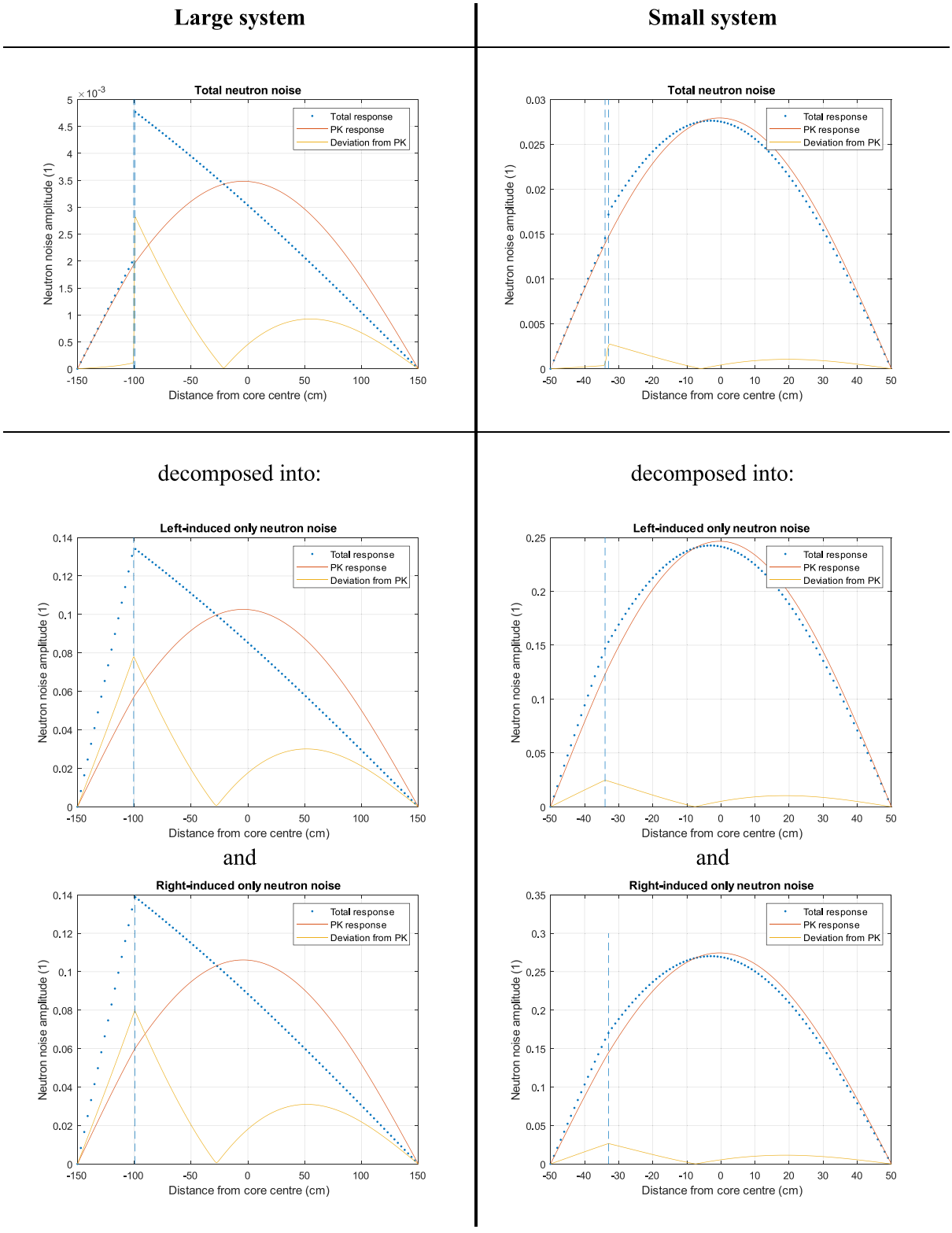

Fig. 10. Analysis of the amplitude of the neutron noise induced by a peripheral perturbation at 1 Hz. The results for the large system are given on the left, whereas the results for the small system are given on the right. The top-row figures give the induced neutron noise, decomposed into the component induced by the vibration of the boundary located in *b* (mid-row figures) and into the component induced by the vibration of the boundary located in *c* (bottom-row figures). "PK" means point-kinetics.

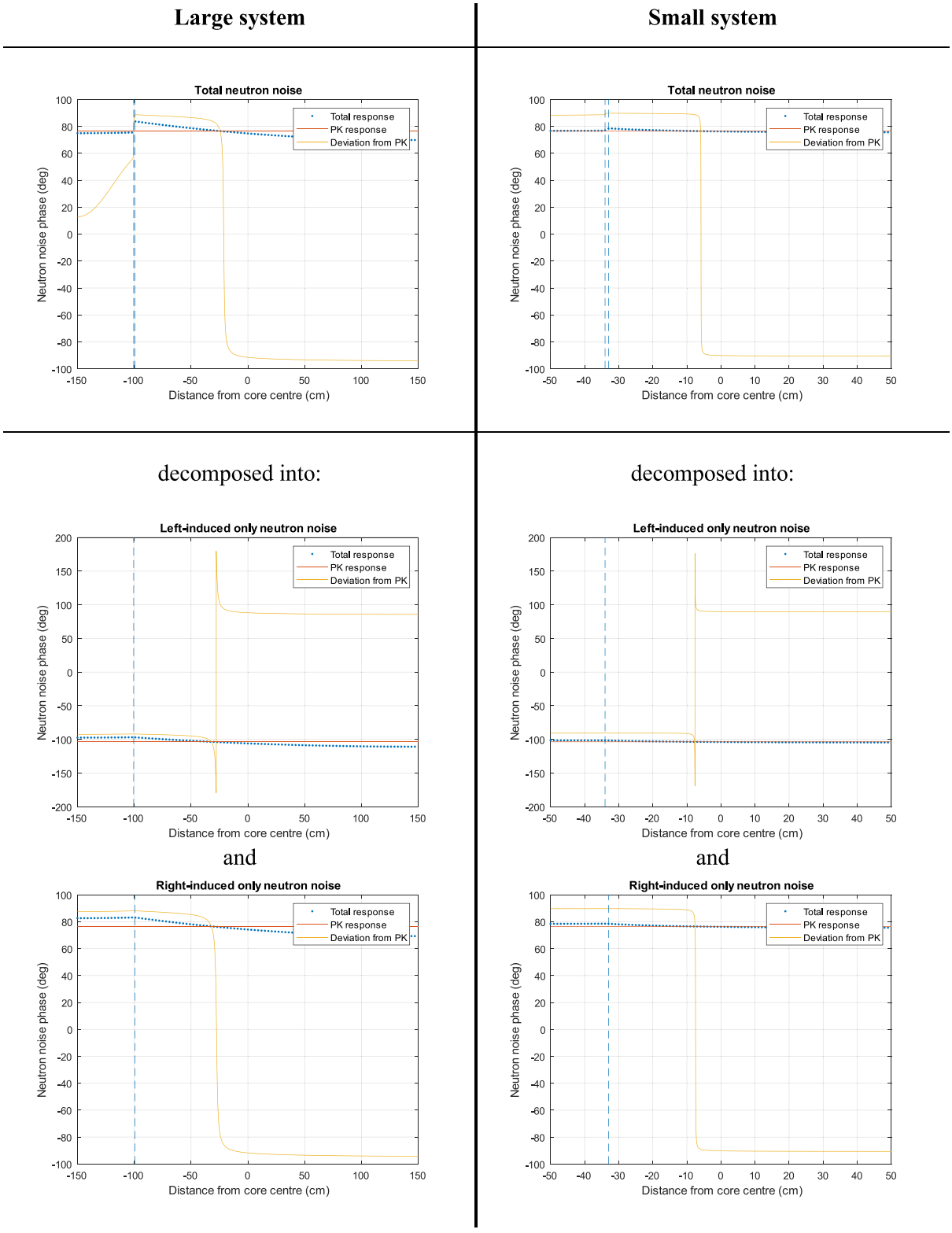

Fig. 11. Analysis of the phase of the neutron noise induced by a peripheral perturbation at 1 Hz. The results for the large system are given on the left, whereas the results for the small system are given on the right. The top-row figures give the induced neutron noise, decomposed into the component induced by the vibration of the boundary located in *b* (mid-row figures) and into the component induced by the vibration of the boundary located in *c* (bottom-row figures). "PK" means point-kinetics.

Although the amplitude of the total neutron noise follows the shape of point-kinetics, the response is everything but point-kinetics. This is also confirmed by the phase of the total neutron noise being purely anti-symmetrical (out-of-phase).

7.2. Case of off-central perturbations

Although the cross-section perturbations given by Eq. (15) and by Eqs. (5)-(7) are symmetrical around the centre of the inner region, there is a tilt in the static neutron flux, resulting in a slightly anti-symmetrical term $\delta S(x',\omega)\phi_0(x')$ in Eq. (10). As a result, the neutron noise induced by the vibrating boundary at *b* and the neutron noise induced by the vibrating boundary at *c* are now slightly anti-symmetrical. This loss of symmetry as compared to the central perturbation leads to the effect of one of the noise sources potentially overwhelming the other one.

This is clearly seen in the total neutron noise as compared to the individual contribution from each of the two vibrating boundaries. This leads to a jump in the amplitude of the total neutron noise between the left part of the moving region and the right part of the moving region. Due to the absence of perfectly anti-symmetrical response as compared to the case of central perturbations, a significant point-kinetics response in the total neutron noise can be observed. This also results in a phase jump in the total neutron noise being much smaller than in the case of central perturbations. Likewise, the point-kinetics component in the small system is much stronger than in the large system, as the result of small systems behaving more in a point-kinetics manner (Pázsit and Demazière, 2010). Along the same line, one notices that the closer the inner region is to the outer boundary, the stronger the point-kinetics response becomes. This is due to the steep gradient of the neutron flux, making $\delta S(x',\omega)\phi_0(x')$ even more anti-symmetrical. This also gives a jump in the phase becoming almost insignificant.

8. Analysis of the neutron noise at the first higher harmonics

The amplitude and phase of the neutron noise induced by the central perturbation are given in Figs. 12 and 13, respectively. The amplitude and phase of the neutron noise induced by the mid-core perturbation are given in Figs. 14 and 15, respectively. The amplitude and phase of the neutron noise induced by the peripheral perturbation are given in Figs. 16 and 17, respectively. In all figures, the results of both the large and small systems are presented. Moreover, the neutron noise induced by the moving inner region is decomposed into the neutron noise induced by the vibration of the boundary located in *b* (referred to as "left-induced only neutron noise" in the figures) and the neutron noise induced by the vibration of the boundary located in *c* (referred to as "right-induced only neutron noise" in the figures).

As can be seen in Fig. 3 for the 2 Hz component, the noise source is represented by perturbations located in *b* and *c*. Contrary to the 1 Hz component, each of the two perturbations is anti-symmetrical (out-of-phase) around its respective static boundary. As a result, each of the two perturbations lead to responses being out-of-phase around their respective static boundary. Nevertheless, at the same time, the perturbations located in *b* and *c* are located at symmetrical positions with respect to the centre of the moving region. This means the neutron noise responses induced by the perturbations located in *b* and *c* are in-phase with respect to the centre of the moving region.

In essence, one can see the noise source at 2 Hz as the superposition of two noise sources equivalent to the ones observed at 1 Hz, with each of the noise sources anti-symmetrical around their respective boundaries, while the two noise sources being symmetrical around the centre of the moving region. When decomposing the induced neutron noise into the effect due to the noise source located in *b* and *c*, respectively, one thus expects that each of the decomposed effect resembles the effect of the noise source at 1 Hz. This is indeed the case when comparing the induced neutron noise at 2 Hz decomposed into the effect due to the noise sources located in *b* and *c*, respectively – bottom part of Figs. 12-17 – to the total induced neutron noise at 1 Hz – top part of Figs. 6-11.

8.1. Case of the central perturbation

As each moving boundary is slightly shifted from the centre of the system, each noise source leads to some significant deviation from point-kinetics, as the reactivity effect given by Eq. (23) is non-zero. The jump in the amplitude of the decomposed induced neutron noise at the position of its respective moving boundary is also the result of the equilibrium boundary not being at the centre of the system – this can be quantitatively compared to the total neutron noise at 1 Hz in case of off-central perturbations, e.g., Figs. 8 and 10. The deviations from point-kinetics for each of the two perturbations are anti-symmetrical, whereas the respective point-kinetics responses are in-phase. As a result, when combining the effects of each of the two moving boundaries, the deviations from point-kinetics essentially compensate each other, thus re-establishing an apparent overwhelming point-kinetics behaviour. The existence of a significant point-kinetics behaviour is also expected from the examination of Eq. (23), for which the total noise source at 2 Hz is depicted in Fig. 3.

It is interesting to notice that the shape of the amplitude of the total neutron noise is similar between 1 Hz and 2 Hz – see top part of Figs. 6 and 12, respectively – whereas the phase is different – out-of-phase behaviour at 1 Hz, as observed in the top part of Fig. 7, as opposed to the in-phase behaviour at 2 Hz, as observed in the top part of Fig. 13. This stems from the response at 1 Hz being a pure deviation from point-kinetics, whereas the response at 2 Hz is an overwhelming point-kinetics response. The latter is due to cancellation effects, re-establishing an apparent point-kinetics response.

As earlier mentioned, small systems tend to behave in a point-kinetics manner. It thus follows that the deviation of the system response from point-kinetics in the small system is completely negligible as compared to the deviation in the large system.

8.2. Case of off-central perturbation

Because of the anti-symmetry in flux gradient existing at the positions of the two moving boundaries, the individual responses, although having the same spatial shape, have slightly different overall amplitudes. Moreover, whereas in the case of central perturbations, the point-kinetics components of the individual responses were in-phase due to the symmetry of the problem, in the case of off-central perturbations, the respective point-kinetics components are out-of-phase. Nevertheless, the difference in respective amplitudes leads to one of the point-kinetics responses dominating over the other one. Equivalently, it can be stated that the subtraction of two point-kinetics components of different amplitudes leads to an overwhelming point-kinetics component. It can also be noticed that the point-kinetics responses associated to each of the two noise sources are significantly higher in the case of off-central perturbations as compared to the case of central perturbations. This is explained by a larger static flux gradient for off-central perturbations, leading to a larger reactivity effect, according to Eq. (23).

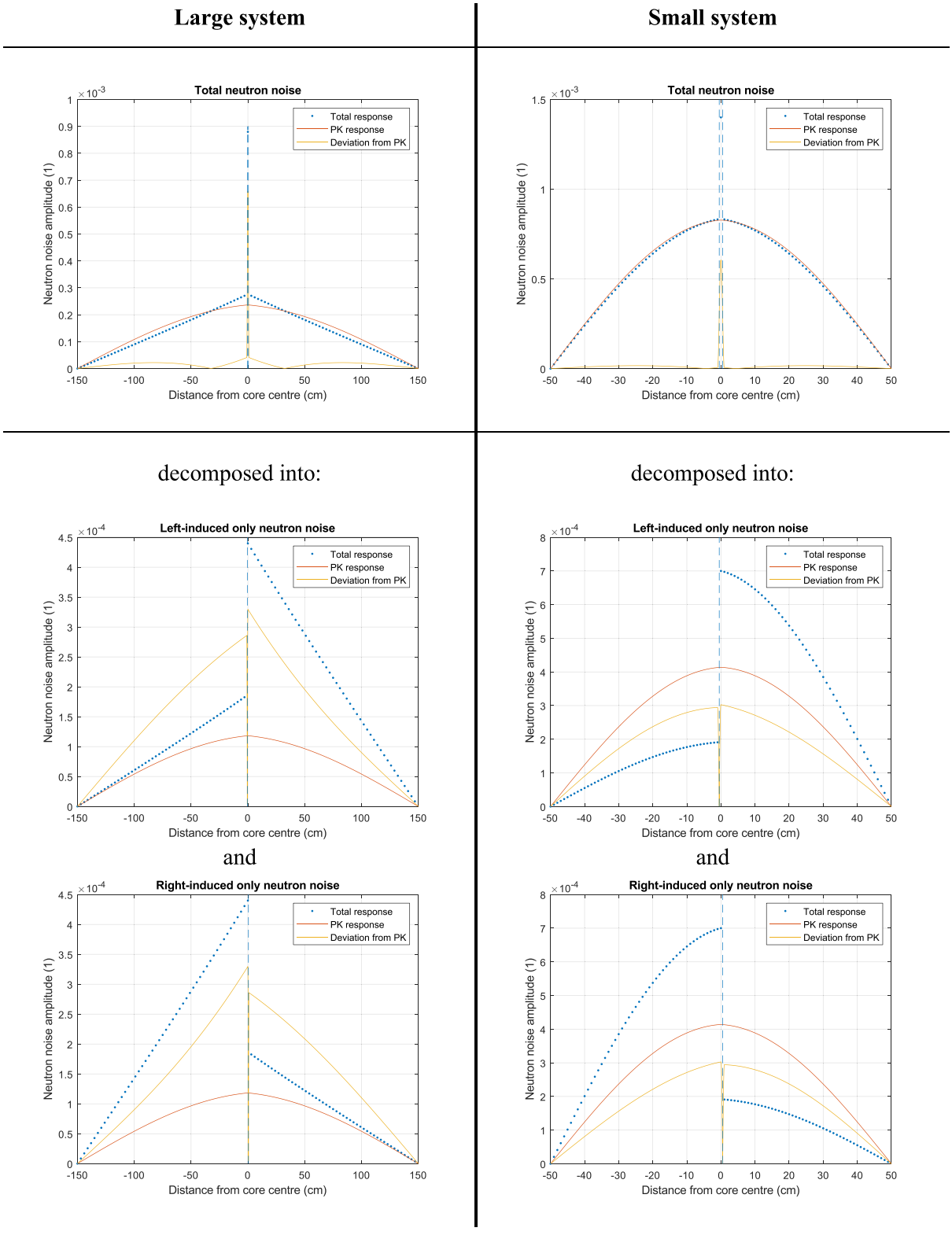

Fig. 12. Analysis of the amplitude of the neutron noise induced by a central perturbation at 2 Hz. The results for the large system are given on the left, whereas the results for the small system are given on the right. The top-row figures give the induced neutron noise, decomposed into the component induced by the vibration of the boundary located in *b* (mid-row figures) and into the component induced by the vibration of the boundary located in *c* (bottom-row figures). "PK" means point-kinetics.

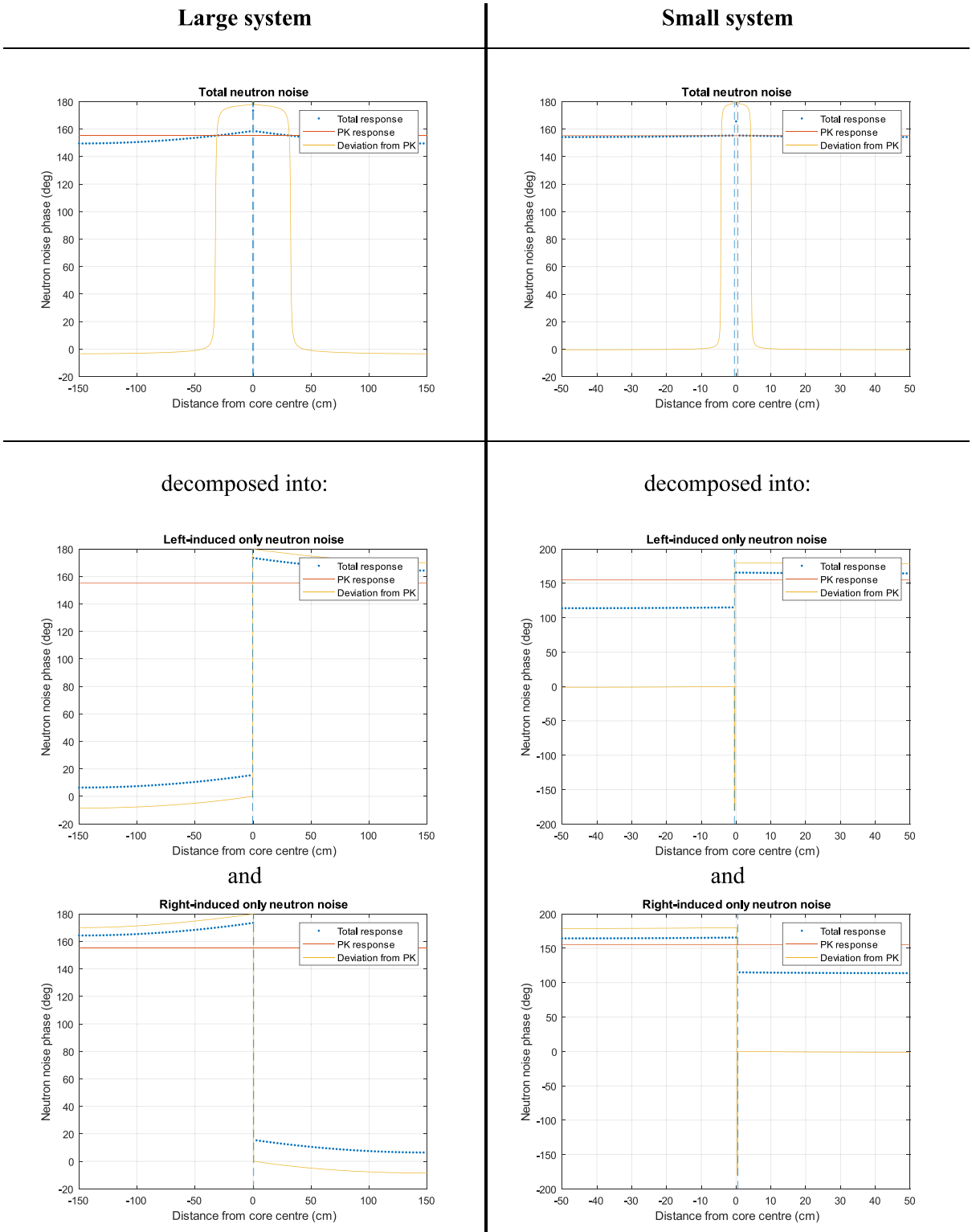

Fig. 13. Analysis of the phase of the neutron noise induced by a central perturbation at 2 Hz. The results for the large system are given on the left, whereas the results for the small system are given on the right. The top-row figures give the induced neutron noise, decomposed into the component induced by the vibration of the boundary located in *b* (mid-row figures) and into the component induced by the vibration of the boundary located in *c* (bottom-row figures). "PK" means point-kinetics.

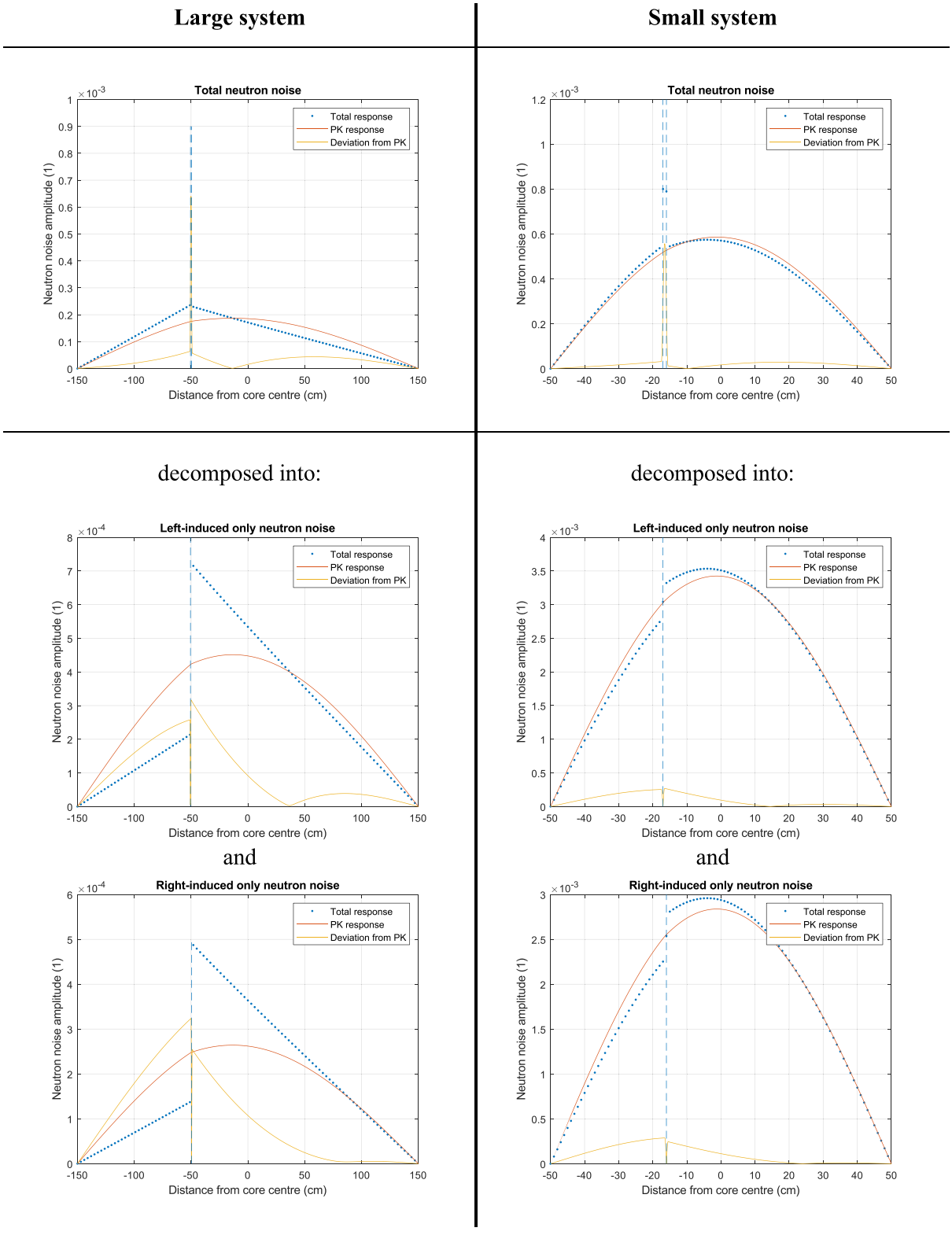

Fig. 14. Analysis of the amplitude of the neutron noise induced by a mid-core perturbation at 2 Hz. The results for the large system are given on the left, whereas the results for the small system are given on the right. The top-row figures give the induced neutron noise, decomposed into the component induced by the vibration of the boundary located in *b* (mid-row figures) and into the component induced by the vibration of the boundary located in *c* (bottom-row figures). "PK" means point-kinetics.

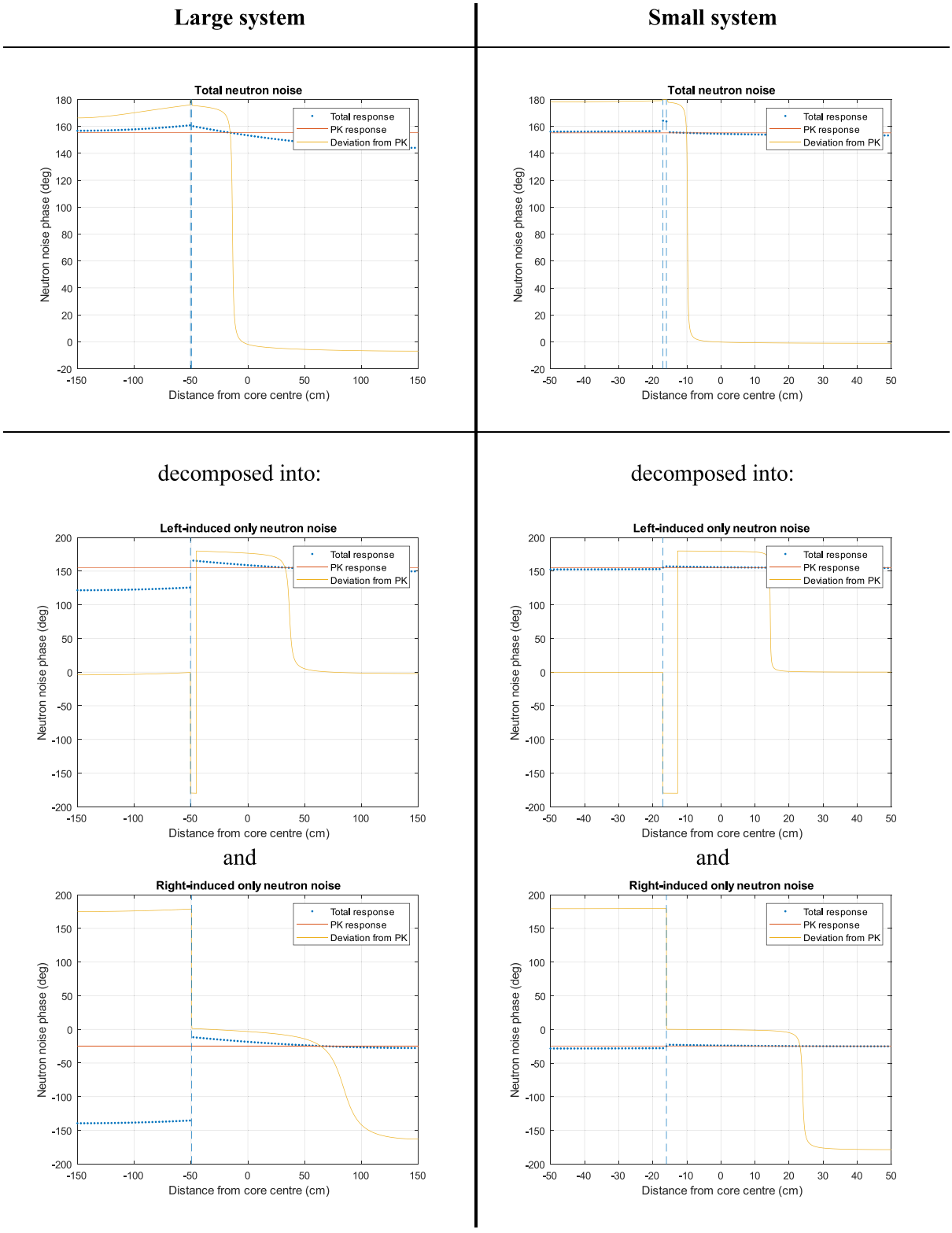

Fig. 15. Analysis of the phase of the neutron noise induced by a mid-core perturbation at 2 Hz. The results for the large system are given on the left, whereas the results for the small system are given on the right. The top-row figures give the induced neutron noise, decomposed into the component induced by the vibration of the boundary located in *b* (mid-row figures) and into the component induced by the vibration of the boundary located in *c* (bottom-row figures). "PK" means point-kinetics.

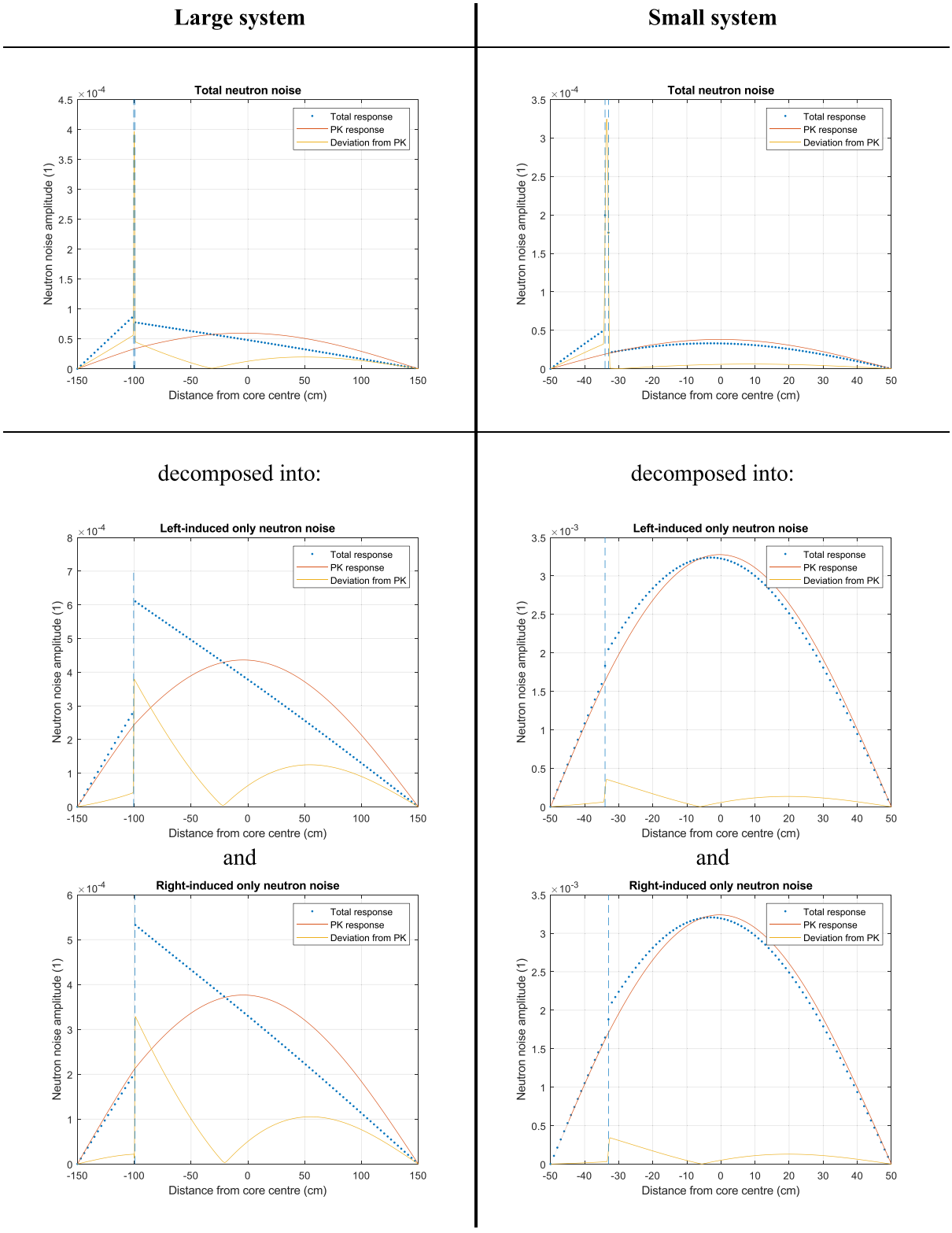

Fig. 16. Analysis of the amplitude of the neutron noise induced by a peripheral perturbation at 2 Hz. The results for the large system are given on the left, whereas the results for the small system are given on the right. The top-row figures give the induced neutron noise, decomposed into the component induced by the vibration of the boundary located in *b* (mid-row figures) and into the component induced by the vibration of the boundary located in *c* (bottom-row figures). "PK" means point-kinetics.

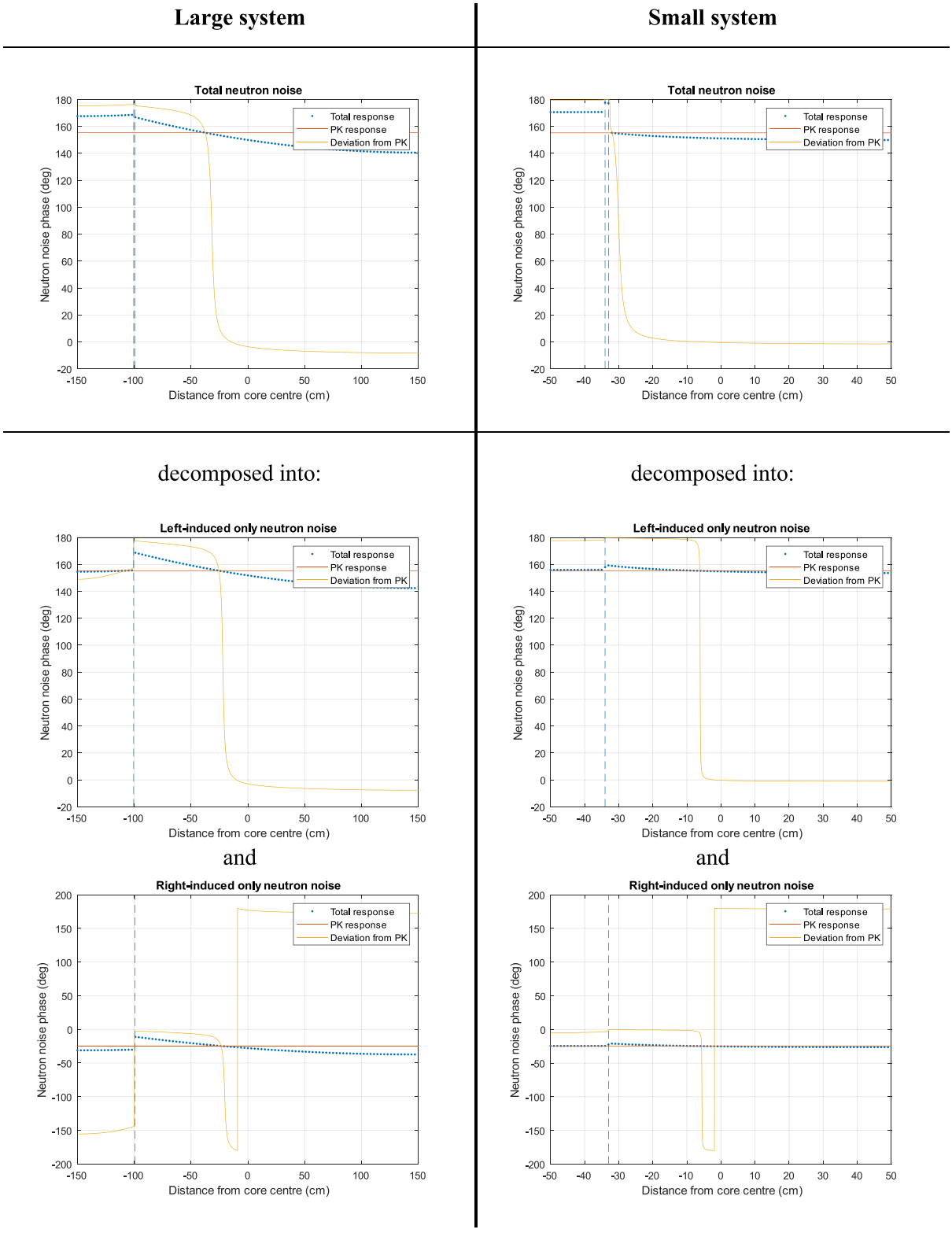

Fig. 17. Analysis of the phase of the neutron noise induced by a peripheral perturbation at 2 Hz. The results for the large system are given on the left, whereas the results for the small system are given on the right. The top-row figures give the induced neutron noise, decomposed into the component induced by the vibration of the boundary located in *b* (mid-row figures) and into the component induced by the vibration of the boundary located in *c* (bottom-row figures). "PK" means point-kinetics.

As earlier noticed, such a point-kinetics component is significantly larger in small systems, as compared to large systems, since small systems tend to behave in a point-kinetics manner.

9. Conclusions

In this paper, the vibrations of an inner region surrounded by two identical regions were considered in one-group diffusion theory, both for a large and a small system. The inner region had a size representative of a fuel pin. It was demonstrated that the vibrations lead to an intricate combination of point-kinetics responses and space-dependent responses associated to each of the moving boundaries. Depending on the position of the moving regions, the harmonics being considered, and the gradient of the static flux, strikingly different responses for the total noise are observed in linear theory.

It is interesting to notice that, although the second harmonic of the neutron noise at 2 Hz seems to have the same shape irrespective of the position of the inner region, the physical mechanisms leading to such apparently identical responses are fundamentally different, with the point-kinetics responses of the individual contributions being in-phase for central perturbations and out-of-phase for off-central perturbations. For the fundamental harmonic of the neutron noise at 1 Hz, on the other hand, the different mechanisms lead to different shapes of the induced neutron noise between central and off-central perturbations. In the special case of central perturbations at 1 Hz, the point-kinetics component of the noise is exactly zero, due to a zero-reactivity effect of the noise source. In all other cases, a significant point-kinetics component in the total neutron noise is present. These findings highlight the importance of the symmetries in the system with respect to the resulting noise field through the core.

At 1 Hz, the neutron noise does not systematically display an out-of-phase behaviour, depending on the relative amplitude of its point-kinetics component.

This work, via dedicated simulations, shed light on the underlying principles leading to such a variety of system responses. Despite the simplicity of the model examined in this paper, the reported results are also important for understanding the neutron noise induced by several fuel pins vibrating in a fuel assembly. In fact, in linear theory, the neutron noise induced by multiple noise sources is given by the superposition of the individual sources. Further studies will investigate interference effects that may exist between the pins.

This work also provides guidance to the analysts on the interpretation of the measured or calculated neutron noise in case of vibrating structures. More specifically, the decomposition of the system response into its point-kinetics response and its deviation from it gives insight into the governing physics, thus enhancing the reliability of the measured or simulated data.

Declaration of Competing Interest

The authors declare that they have no known competing financial interests or personal relationships that could have appeared to influence the work reported in this paper.

Acknowledgements

The research conducted was made possible through funding from the Euratom research and training programme 2014-2018 under grant agreement No 754316 (CORTEX project).

References

Bell, G., Glasstone, S., 1970. Nuclear reactor theory. Van Nostrand Reinhold Company, New York, USA.

Bläsius, C., 2018. Private communication. Gesellschaft für Anlagen- und Reaktorsicherheit (GRS) gGmbH.

Brighenti, A., Santandrea, S., Zmijarevic, I., Stankovski, Z., 2022. Development and validation of a time-dependent deterministic model for neutron noise on CROCUS experimental measurements. Ann. Nucl. Energy 165, 108753. https://doi.org/10.1016/j.anucene.2021.108753.

Demazière, C., 2011. CORE SIM: A multi-purpose neutronic tool for research and education. Ann. Nucl. Energy 38 (12), 2698–2718. https://doi.org/10.1016/j.anucene.2011.06.010.

Demazière, C., Vinai, P., Hursin, M., Kollias, S., Herb, J., 2018. Overview of the CORTEX project. In: Proc. Int. Conf. Physics of Reactors – Reactor Physics paving the way towards more efficient systems (PHYSOR2018), Cancun, Mexico, April 22-26, 2018.

Demazière, C., Dokhane, A., 2019. Description of scenarios for the simulated data. CORTEX deliverable D3, 1.

Durrant, A., Leontidis, G., Kollias, S., Torres, L.A., Montalvo, C., Mylonakis, A., Demazière, C., Vinai, P., 2021. Detection and localisation of multiple in-core perturbations with neutron noise-based self-supervised domain adaptation. American Nuclear Society.

Jonsson, A., Tran, H.N., Dykin, V., Pázsit, I., 2012. Analytical investigation of the properties of neutron noise induced by vibrating absorber and control rods. Kerntechnik 77 (5), 371–380.

Lamirand, V., Rais, A., Hübner, S., Lange, C., Pohlus, J., Paquee, U., Pohl, C., Pakari, O., Frajtag, P., Godat, D., Hursin, M., Laureau, A., Perret, G., Fiorina, C., Pautz, A., Lyoussi, A., Giot, M., Carette, M., Jenčič, I., Reynard-Carette, C., Vermeeren, L., Snoj, L., Le Dû, P., 2020. Neutron noise experiments in the AKR-2 and CROCUS reactors for the European project CORTEX. EPJ Web of Conferences 225, 04023. https://doi.org/10.1051/epjconf/202022504023.

Pázsit, I., Karlsson, J., 1997. On the perturbative calculation of the vibration noise by strong absorbers. Ann. Nucl. Energy 24 (6), 449–466. https://doi.org/10.1016/S0306-4549(96)00081-3.

Pázsit, I., Demazière, C., 2010. In: Handbook of Nuclear Engineering. Springer US, Boston, MA, pp. 1629–1737. https://doi.org/10.1007/978-0-387-98149-9_14.

Rouchon, A., Sanchez, R., 2015. Analysis of vibration-induced neutron noise using one-dimension noise diffusion theory. In: Proc. Int. Congress Advances in Nuclear Power Plants (ICAPP2015), Nice, France, May 3-5, 2015.

Seidl, M., Kosowski, K., Schüler, U., Belblidia, L., 2015. Review of the historic neutron noise behavior in German KWU built PWRs. Prog. Nucl. Energy 85, 668–675. https://doi.org/10.1016/j.pnucene.2015.08.016.

Thie, J.A., 1981. Power reactor noise. American Nuclear Society, La Grange Park, Illinois, USA.

Verma, V., Chionis, D., Dokhane, A., Ferroukhi, H., 2021. Studies of reactor noise response to vibrations of reactor internals and thermal-hydraulic fluctuations in PWRs. Ann. Nucl. Energy 157, 108212. https://doi.org/10.1016/j.anucene.2021.108212.

Vidal-Ferràndiz, A., Carreño, A., Ginestar, D., Demazière, C., Verdú, G., 2020a. A time and frequency domain analysis of the effect of vibrating fuel assemblies on the neutron noise. Ann. Nucl. Energy 137, 107076. https://doi.org/10.1016/j.anucene.2019.107076.

Vidal-Ferràndiz, A., Carreño, A., Ginestar, D., Demazière, C., Verdú, G., 2020b. Neutronic simulation of fuel assembly vibrations in a nuclear reactor. Nucl. Sci. Eng. 194 (11), 1067–1078. https://doi.org/10.1080/00295639.2020.1756617.

Vidal-Ferràndiz, A., Demazière, C., Dokhane, A., Ginestar, D., Knospe, A., Kuentzel, M., Mylonakis, A., Périn, Y., Lange, C., Verdú, G., Verma, V., Vinai, P., 2020c. Modelling of the neutron flux response to vibrating fuel assemblies. CORTEX deliverable D1, 3.

Viebach, M., Lange, C., Bernt, N., Seidl, M., Hennig, D., Hurtado, A., 2019. Simulation of low-frequency PWR neutron flux fluctuations. Prog. Nucl. Energy 117, 103039. https://doi.org/10.1016/j.pnucene.2019.103039.

Vinai, P., Brighenti, A., Demazière, C., Gasse, B., Ginestar, D., Mylonakis, A., Rouchon, A., Santandrea, S., Tatidis, A., Vidal-Ferràndiz, A., Verdú, G., Yamamoto, T., Yi, H., Zmijarevic, I., Zoia, A., 2021a. Development and comparison of high-order solvers for reactor noise analysis. CORTEX deliverable D1, 4.

Vinai, P., Ambrozic, K., Brighenti, A., Demazière, C., Gasse, B., Ginestar, D., Hursin, M., Hübner, S., Knospe, A., Lamirand, V., Lange, C., Laureau, A., Macian, R., Mylonakis, A., Pakari, O., Rais, A., Rouchon, A., Santandrea, S., Stankovski, Z., Verdú, G., Vidal-Ferràndiz, A., Yamamoto, T., Yi, H., Yum, S., Zmijarevic, I., Zoia, A., 2021b. Final validation report. CORTEX deliverable D2, 5.

Vinai, P., Yi, H., Mylonakis, A., Demazière, C., Gasse, B., Rouchon, A., Zoia, A., Vidal-Ferràndiz, A., Ginestar, D., Verdú, G., Yamamoto, T., 2021. Comparison of neutron noise solvers based on numerical benchmarks in a 2-D simplified UOX fuel assembly. In: Proc. Int. Conf. Mathematics and Computational Methods Applied to Nuclear Science and Engineering (M&C2021), Raleigh, North Carolina, USA, October 3-7, 2021. https://dx.doi.org/10.13182/M&C21-33625.

Zoia, A., Rouchon, A., Gasse, B., Demazière, C., Vinai, P., 2021. Analysis of the neutron noise induced by fuel assembly vibrations. Ann. Nucl. Energy 154, 108061. https://doi.org/10.1016/j.anucene.2020.108061.